Journal of Optoelectronics and Advanced Materials Vol. 5, No. 2, June 2003, p. 447 - 477

EFFECT OF LOSS AND PULSE WIDTH VARIATION ON SOLITON PROPAGATION

Part I. Fundamentals of soliton propagation

M. S. Ozyazici*, M. Sayin

Department of Electrical and Engineering, University of Gaziantep,
27310-Gaziantep, Turkey

In this work, the propagation of solitons in single-mode optical fibers has been investigated theoretically by using the nonlinear Schrödinger equation. This equation combines the effects of group velocity dispersion and self-phase modulation present in optical fibers and also takes into account the loss of optical fiber. The nonlinear Schrödinger equation has been solved numerically by using the split-step Fourier transform technique. In particular, soliton solutions of this equation are obtained. Computer simulations depicting the propagation of solitons having picosecond pulse widths, over several tens of kilometers in optical fibers with losses are presented. The results obtained for solitons in the lossless case demonstrate the shape-preserving property of the first order soliton and periodicity, splitting and compression properties of higher order solitons. Computer simulations show that the optical loss broadens the pulse width of solitons and increases the soliton period. However, this broadening in the pulse width is directly proportional to the optical loss unlike broadening effect of dispersion. It has found that the use of solitons in optical communication systems can improve the bit-rate over the same distance of propagation compared to normal optical communication systems even if no precaution is taken against the pulse broadening effect due to loss.

(Received April 17, 2003, accepted May 8, 2003)

Keywords: Soliton, Optical fiber, Optical loss, Optical communication system

1. Introduction

In the early stage of optical fiber development, much of the effort was devoted to decreasing the loss which attenuates the optical signal after a certain propagation length to a value below the detection limit of detectors and hence puts an upper limit to the distance that the signal can be transmitted without repeaters. These efforts led to the realization of the low-loss single-mode silica fiber, which has a minimum attenuation at 1.55 μm [1]. However, a critical obstacle in achieving the full bandwidth capacity of optical fiber communication systems is pulse spreading which arises from the dispersive nature of the fiber material [2]. Dispersion, which is the manifestation of the wavelength dependence of the mode group velocity (group velocity dispersion), causes the pulses spread out and eventually overlap to such an extent that all information has been lost. In digital transmission, this places an upper limit, for a given transmission distance, on the rate at which pulses can be sent. The combined effects of dispersion and loss have thus far made it possible to use only a small fraction of the tremendous bandwidth of optical fiber. In single-mode fibers, the total dispersion is the sum of material dispersion caused by the dispersive properties of the waveguide material and

*Corresponding author: sadi@gantep.edu.tr

waveguide dispersion caused by the guidance effects within the fiber structure [3]. The total dispersion can be negative or positive depending on working wavelength. In silica based fibers, the total dispersion passes through zero around 1.3 μm and it is negative (anomalous dispersion) for the wavelength greater than 1.3 μm [4].

In 1973, Hasegawa and Tappert [5,6] modeled the propagation of coherent optical pulses in optical fibers by nonlinear Schrödinger equation (NLS). They showed theoretically that generation and propagation of shape-preserving pulses called solitons, in optical fibers, are possible by balancing the dispersion of optical fibers with the small non-linearity of the fiber's intensity-dependent refractive index. Hasegawa and Tappert numerically solved the NLS equation. This equation has an exact solution for an initial pulse shape of *Nsech(t)* where N is any integer ≥1, known as the order of the soliton [7,8]. The first order soliton is a self-maintaining pulse, whereas higher order solitons split and narrow, recovering their initial shape at the end of a period which is $\pi/2$ in the normalized coordinate axis. This period is known as the soliton period and is a function of pulse width, dispersion and wavelength. Hasegawa and Tappert [5,6] showed that the pulses can be convex upward (bright solitons) or concave upward (dark solitons) depending on the sign of the dispersion. If dispersion is negative (anomalous dispersion), the solution of the NLS equation supports bright solitons since they consist of a stable intense pulse of light moving against a dark background. If dispersion is positive (normal dispersion), dark solitons are generated since they consist of an illuminated background supporting an intense propagating hole. The possibility of the generation of both types of solitons has been shown by Hasegawa and Tappert, and later by other researchers [9-11]. The following properties of solitons make them attractive for optical communication systems:

1. pulse shape, the width and speed are preserved in the absence of loss;
2. solitons are stable against small perturbations;
3. they collide with each other without changing their shape and speed;
4. they can be view as the common asymptotic state of completely different initial pulses.

At present, soliton propagation is the only method, which can eliminate dispersion: induced broadening of pulses in fiber-optic transmission. This important discovery of Hasegawa and Tappert stimulated extended research towards shape-preserving optical solitons as information carrying entities in high bit-rate optical fiber communication systems.

The ideas of Hasegawa and Tappert could not be supported by experiments since neither low-loss single-mode optical fiber nor a suitable mode locked laser delivering high peak power picosecond pulses at the correct wavelength was available. With advance of fiber optic and laser technology, Mollenauer and co-workers performed a remarkable experiment in 1980 and demonstrated the generation of optical solitons in single-mode optical fibers [12]. They explained the soliton generation mechanism in optical fibers in the following way [12-14]: The intensity-dependent refractive index in optical fibers can cause a phenomenon known as self-phase modulation [15]. Self-phase modulation modulates the phase of the optical carrier, that it normally increases the frequency in the trailing part of the pulse and decreasing the frequency in the leading part. The modification of pulse structure in this way is known as chirping and the overall effect is to broaden the spectrum. Dispersion in optical fibers always causes pulse broadening irrespective of its sign. The sign of the dispersion only determines which parts of the pulse are retarded or advanced compared to other parts. Since trailing part of the pulse contains higher frequencies, this part of the pulse will propagate faster than the leading part if dispersion of fiber is negative. Hence, the back of the pulse catches up the front part and the pulse tends to narrow. Depending on the amount of chirp generated in the fiber, the propagating pulse will either keep its shape or be compressed. In this way, dispersion, which on its own causes the pulses to broaden, leads to compressed or shape-preserving pulses in optical fibers. Although the explanation given above illustrates pulse compression optical fiber in a simplified manner, it does not predict other pulse shaping effects such as splitting, interaction, periodicity and the effect of loss on pulse width. In order to show the latter effects, one should solve (numerically) the appropriate NLS equation with suitable initial conditions.

In this work, the NLS equation with an added term representing optical loss is numerically solved for solitons by using the split-step Fourier transform technique. In particular, the effect of loss on the pulse width of solitons having initial pulse width of a few picosecond propagating over several tens of kilometers in optical fiber with losses is investigated.

2. Mathematical model

The equation governing the propagation of picosecond pulses under the combined effects of self-phase modulation and dispersion of optical fiber is given by [16]

$$j\left(\frac{\partial\phi}{\partial z}+\gamma\phi+\beta_o'\frac{\partial\phi}{\partial t}\right)+\frac{\left|\beta_o''\right|}{2}\frac{\partial^2\phi}{\partial t^2}+\frac{n_2\omega_o}{4c}\left|\phi\right|^2\phi=0 \tag{1}$$

where ϕ is the complex slowly-varying envelope function, γ is the optical loss, ω_o is the radian frequency, β'_o is the inverse of the group velocity at ω_o, β''_o is the total dispersion at ω_o, c is the speed of light, t is the time, z is the distance and n_2 is the coefficient of the intensity-dependent refractive index. The first step in solving a nonlinear differential equation is to transform it into dimensionless coordinates by using suitable transformations. The following transformations will be used for eq. (1),

$$s=\frac{1}{t_c}\left(t-\beta_o'z\right) \tag{2}$$

$$\zeta=\frac{\left|\beta_o''\right|z}{t_c^2} \tag{3}$$

$$u=t_c\left(\frac{n_2\omega_o}{4c\left|\beta_o''\right|}\right)^{1/2}\phi \tag{4}$$

where s is the coordinate moving with a group velocity (dimensionless retarded time variable) and t_c is an arbitrary time scale. The time scale t_c in this transformation allows a pulse of standard duration in the dimensionless variable s to correspond to a pulse of any desired duration in time t. These transformations will later be used to find the soliton period and the fundamental soliton power linking the physical parameters with the dimensionless parameters. Equation (1) is transformed into dimensionless coordinates by using the above transformations as

$$j\frac{\partial u}{\partial\zeta}+\frac{1}{2}\frac{\partial^2u}{\partial s^2}+\left|u\right|^2u=-j\Gamma_l u \tag{5}$$

where Γ_l is equal to $\gamma t_c/\left|\beta''_o\right|$.

If the term representing the loss of the optical fiber is omitted from the right hand side of eq. (5), this equation is called nonlinear Schrödinger (NLS) equation. The NLS equation can be solved exactly by using the inverse scattering theorem [7,8], and supports soliton solutions which are ideally suited to the representation of digital signals and have desirable property that they do not suffer from dispersion. For an input pulse of the form

$$u(0, s) = \mathrm{N}\,\mathrm{sech}(s) \tag{6}$$

where N is an integer known as the order of the soliton, the analytical solutions of the NLS equation for N=1, 2 are given [7,8] by

$$u_1(\zeta, s) = e^{-j\zeta/2}\,\mathrm{sech}\,(s) \tag{7}$$

$$u_2(\zeta,s)=\frac{4e^{-j\zeta/2}\left[\cosh(3s)+3e^{-j4\zeta}\cosh(s)\right]}{\left[\cosh(4s)+4\cosh(2s)+3\cos(4s)\right]} \tag{8}$$

The first order soliton given by equation (7) has a magnitude of $\mathrm{sech}^2(s)$ which is independent of ζ. This means that the first order soliton keeps its initial shape during propagation through the optical fiber. However, the magnitude of the second order soliton is not independent of ζ and develops a periodical structure. The period of oscillation which is the same for all solitons is given by $\zeta = \pi/2$. The evolution of higher-order solitons is symmetric at about $\zeta = \pi/4$. For N>2, the solution of the NLS equation become lengthier and no analytic solution are given.

The soliton period and the fundamental power (peak power) are the important quantities for soliton propagation in optical fibers. The fundamental power is the power required within the fiber in order to obtain the first order soliton. Since solitons are periodic in the dimensionless coordinate ζ with a period of $\pi/2$, the soliton period can be obtained from eq. (3) by substituting $\zeta = \pi/2$ and using the relation $t/t_c = 2\cosh^{-1}\sqrt{2} = 1.76$ as

$$Z_o = 0.322\frac{\pi^2 c\tau}{D\lambda^2} \tag{9}$$

where D is the dispersion of the optical fiber, τ is the FWHM of the pulse, c is the speed of light and is the wavelength. The power carried by electromagnetic wave is given by

$$P=\frac{1}{2}n_o\varepsilon_o cA_g\left|\phi\right|^2 \tag{10}$$

where A_g is the geometrical core area of the fiber. Using eq. (4) and eq. (9) in eq. (10), the fundamental power can be obtained as

$$P_o=\frac{\lambda\varepsilon_o cn_o A_g}{2Z_o n_2} \tag{11}$$

Equations (9) and (11) show that the only variable parameters are the pulse duration and the dispersion of the fiber. Once the operating wavelength is fixed, the dispersion of the fiber can no longer be changed. Hence, the only way to change the soliton period and, in turn, the fundamental power is to change the pulse duration. For fiber parameters of D = 16 ps/nm/km at 1.55 μm, d = 8 μm, n_o = 1.46 and $n_2 = 1.22\times10^{-22}$ m^2/V^2, the soliton period and the fundamental power for an input pulse duration of 25 ps are calculated as 16 km and 80 mW, respectively. If the fiber is not polarization preserving, the fundamental power should be increased by a factor of 6/5. For higher-order solitons the power scales with the soliton number and can be written as

$$P_N = N^2 P_o \text{ for } N \geq 2 \tag{12}$$

The soliton period and the fundamental power are plotted in Fig. 1 as a function of the pulse duration for four different values of the fiber dispersion. In the calculations, n_2 is replaced by n_2 5/6 for nonpolarization-preserving fiber. At a fixed value of the pulse duration, the soliton period increases, which in turn decreases the fundamental power if changing the operating wavelength of the system decreases the dispersion of the fiber.

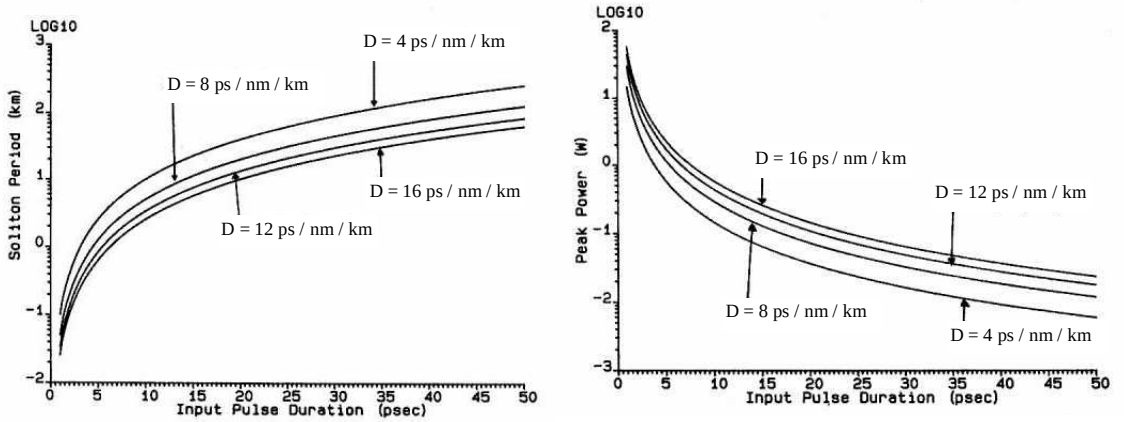

Fig. 1. Soliton period and fundamental power versus input pulse duration for $\lambda = 1.55$ μm and D = 4, 8, 12 and 16 ps/nm/km.

A continuous set of solutions can be generated from the solutions of the NLS equation by using the invariance of the NLS equation. Equation (5) is invariant under the following transformations:

$$\begin{aligned} u' &= Ku \\ \zeta' &= K^{-2}\zeta \\ s' &= K^{-1}s \end{aligned} \tag{13}$$

Therefore, if the soliton amplitude is increased by a factor of *K*, K2 reduces the distance of transmission, K reduces the period, while K2 effectively increases the fiber loss. This scaling law shows that one computation can be reinterpreted for different power levels. For example, in solving eq. (5) for an initial pulse of $|u_{max}| = 1$, if the pulse is found to contract to a width of τ_1 at a distance ζ_1 with the assumed loss rate Γ_{l1}, then an identical process occurs for an initial pulse having amplitude four times greater than the previous one at a distance $\zeta_1/4$ with the pulse width $\tau_1/2$ if the transmission loss rate is four times that assumed in the computation.

3. Split-step Fourier transform method and its application to the numerical solution of the PNLS equation

There are several computational techniques by which one could predict the results of plane wave propagation in a material, which is both nonlinear and dispersive. The dispersive part of the problem involves finding the proper phase shift for each Fourier component, while the nonlinearity is governed by a temporal equation. A particularly simple and general numerical method, the so-called split-step Fourier method (or beam propagation method) has been developed by Hasegawa and Tappert [5,6] to solve the NLS equation for solitons. The split-step Fourier technique has been widely used in analyzing pulse propagation in optical fibers [18,19].

The basic philosophy behind the split-step Fourier technique is to treat the effects of dispersion and nonlinearity, separately. The advantage of this technique is that dispersion is calculated in the frequency domain and nonlinearity in the time domain, both effects requiring only simple multiplication in their own domain. The details of this technique are given in [20-22]. Therefore, the technique is applied directly to the PNLS equation given by eq. (5). The PNLS equation is written formally as

$$\frac{\partial u}{\partial \zeta} = (X + Y)\,u \tag{14}$$

where the differential operator X includes a term involving dispersion and Y consists of the nonlinear term and the loss term. These operators can be written from eq. (5) as

$$X\left[\frac{\partial}{\partial s}\right]=\frac{j}{2}\frac{\partial^2}{\partial s^2} \tag{15}$$

$$Y(u)=j|u|^2-\Gamma_l \tag{16}$$

An exact solution is difficult to obtain because of the non-commuting nature of the operators *X* and *Y*. However, an approximate solution can be obtained using the following symmetrized split-step procedure [20-22] to propagate the complex field *u (z,s*) by a small distance δ:

$$u(\zeta+\delta,s)=\left\{e^{\delta X/2}\exp\left[\int_{\zeta}^{\zeta+\delta}Y(\zeta')\,d\zeta'\right]e^{\delta X/2}\right\}u(\zeta,s) \tag{17}$$

Symmetrized splitting of operators reduces the commutation error further [20]. The numerical technique consists of propagating the complex field for a distance δ/2 with dispersion only by setting $Y = 0$, multiplying the result by a nonlinear term that represents the effect of the nonlinearity and the loss over the whole segment δ, and then propagating the complex field for the remaining distance δ/2 with dispersion only. The error is minimized when the effect of nonlinearity is included in the midplane rather than in the beginning or the end of a segment [21]. Further, the error decreases as the magnitude of δ decreases, and sufficiently accurate results can be obtained with a proper choice of the step size δ.

The propagation of pulses in a linear dispersive medium governed by the exponential term exp (δ*X*/2) in eq. (17) can be easily solved by using the Fourier transform technique. So, the solution of this part of the problem can be written as

$$u(\zeta+\delta/2,s)=exp(\delta G/2)u(\zeta,s)=\left\{F^{-1}\,exp\left[\frac{\delta}{2}G(j\omega)\right]F\right\}u(\zeta,s) \tag{18}$$

where F denotes the Fourier transform operation, $G(j\omega)$ is obtained using eq. (15), and is the Fourier transform variable in the frequency space. The use of the fast Fourier transform algorithm makes numerical evaluation of eq. (18) relatively fast. Eq. (17) can be used repeatedly to propagate the optical pulse through a given length of fiber after suitably choosing the step size δ.

The integral appearing in eq. (17) should be performed carefully. This integral can be approximated by using the trapezoidal rule as

$$\int_{\zeta}^{\zeta+\delta}Y(\zeta')d\zeta'=[Y(\zeta)+Y(\zeta+\delta)]\frac{\delta}{2} \tag{19}$$

where Y(ζ) is given by eq. (16). However, $Y(\zeta+\delta)$ cannot be evaluated since $u(\zeta+\delta,s)$ is not known while evaluating eq. (19) at the midsegment located at ζ+δ/2. Thus, a self-consistent calculation must be done. An iterative procedure was used that was initiated by replacing $Y(\zeta+\delta)$ with $Y(\zeta)$ in eq. (19). Then, eq. (17) was used to estimate $u(\zeta+\delta,s)$ which in turn was used to calculate the new value of $Y(\zeta+\delta)$. In the calculations, two iterations were sufficient to give an overall accuracy of 10^{-5}. The calculations were also performed with reduced step size (without self-consistent technique)

and were found that the program using the self-consistent method was twice as fast as the one with the smaller step size, for the same overall accuracy. In the computer simulation, the step size Δs, which is chosen as 32/1024 was kept the same all the time. The complex field $u(\zeta,s)$ was propagated along the fiber under the effect of dispersion, nonlinearity and loss by using the above procedure and the initial condition of eq. (6).

Using the first conservation law among many of eq. (5) without the right hand side checked the accuracy of the numerical method. The first conserved law of eq. (5) related to the total energy i.e. the number of photons carried by the pulse is given [7] by

$$\int_{-\infty}^{\infty} |u(\zeta, s)|^2 ds = 2N^2 \tag{20}$$

This quantity was checked for the proper choice of the integration step size δ to give an overall accuracy of 10^{-5} in the absence of the loss. In addition, the accuracy of the method was also checked in the presence of the loss. Perturbation analysis of the PNLS equation indicates that the total energy in the pulse decays as $\exp(-2\Gamma_l \zeta)$ [23]. Hence, the total energy can be computed by using the following equation:

$$E_t = 2N^2 e^{-2\Gamma_l \zeta} \tag{21}$$

For the same step size, an overall accuracy of 10^{-4} was obtained between the numerically calculated energy and the one computed from eq. (21) in the presence of the loss.

4. The results of the mathematical model

The propagation of solitons through a single-mode fiber at 1.55 μm is simulated by using the mathematical model explained before. Silica based single-mode fiber having a core diameter of 8 μm, a loss of 0.35 dB/km at 1.55 μm, core refractive index of 1.46, nonlinear coefficient of 1.22×10^{-22} m^2/V^2 and chromatic dispersion of 16 ps/nm/km is used in the computer simulation. The initial pulse width of the sech pulse is chosen as 25 ps, which can easily be generated from semiconductor lasers. This pulse width sets the soliton period and the fundamental power for the nonpolarization-preserving fiber to 16 km and 96 mW (80 mW for polarization-preserving fiber), respectively. Although the results of the computer simulation is depicted for the above pulse and fiber parameters, the same results are applicable to the other pulses with different parameters if the parameters are rescaled by using eq. (13).

4.1 First, second and higher-order solitons

The propagation of solitons through the optical fiber is considered without the optical loss. Fig. 2 represents the first order (N=1) and the second order (N=2) soliton at a half period of $\pi/4$ (8 km). The shape of the first order soliton is exactly same as the input pulse while the second order soliton develops three peaks at the half period. The central peak is the dominant peak and represents a compressed pulse having a pulse width, which is ¼ of the initial pulse width. This suggests that higher-order solitons can be used to compress the pulses to a shorter width. In order to see how the pulse shape changes during the propagation, three-dimensional graphs of the first order and the second order solitons are plotted in Fig. 3 for the entire period.

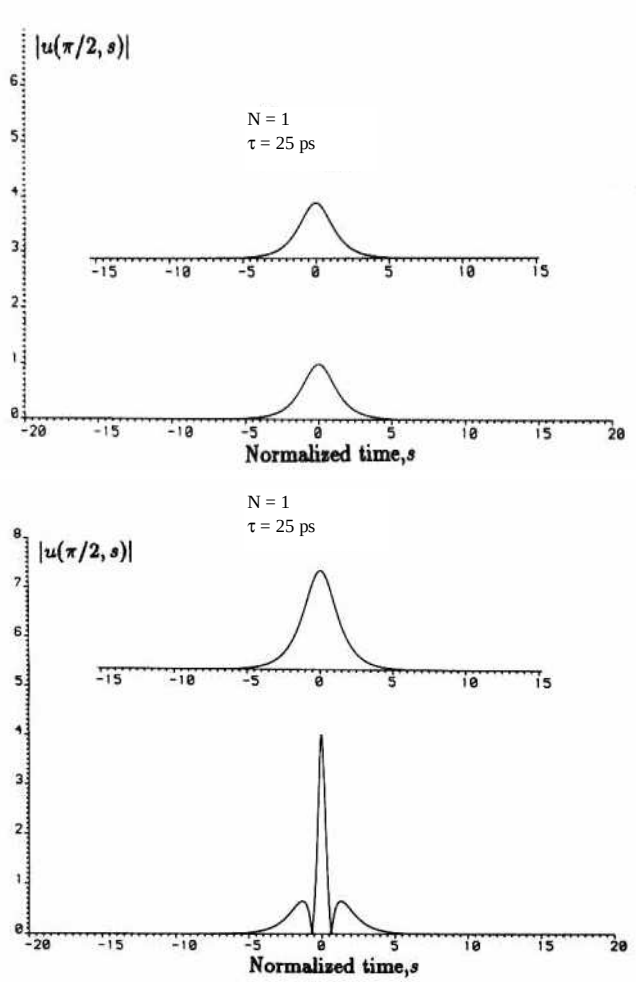

Fig. 2. First and second order solitons at half period (Γ_l =0).

The first order soliton is the only soliton which keeps its initial shape (sech) all the time during the propagation through any length of the fiber. The first order soliton represents the exact balance between the pulse narrowing effect of SPM and the pulse broadening effect of dispersion alone. Thus, the pulse shape and the amplitude are such that the last two terms of eq. (5) cancel completely. This exact balance results in the equation $\partial u/\partial\zeta$ =0. Any deviation from this balance results either in pulse broadening (N<1) or in pulse compression (N>1). This shape-preserving property of the first order soliton makes it ideal for designing high bit-rate and long-distance optical communication systems. However, the above picture is true for the lossless case. The inclusion of loss completely changes the picture, which will be explained later in Section 4.2. The first order soliton requires less power than higher-order solitons, so the first order soliton should be the easiest to generate with semiconductor lasers. The periodic nature of the second order soliton can be seen from Fig. 3. After compressing at the half period, the second order soliton reexpands to its original form developing no further structure.

If the soliton order is increased further, the pulse develops more and more structure at the half period. Fig. 4 represents some higher-order solitons (N=3, 4 and 5). For example, the third order soliton has four peaks at the half period. The number of peaks at the half period is equal to N+1 for N>1. All these peaks where higher-order solitons develop lie within the original pulse width. All higher-order solitons are periodic having same period of $\pi/2$ in dimensionless coordinate ζ. The periodic nature of the some higher-order solitons are depicted in the three dimensional graphs of Fig. 5.

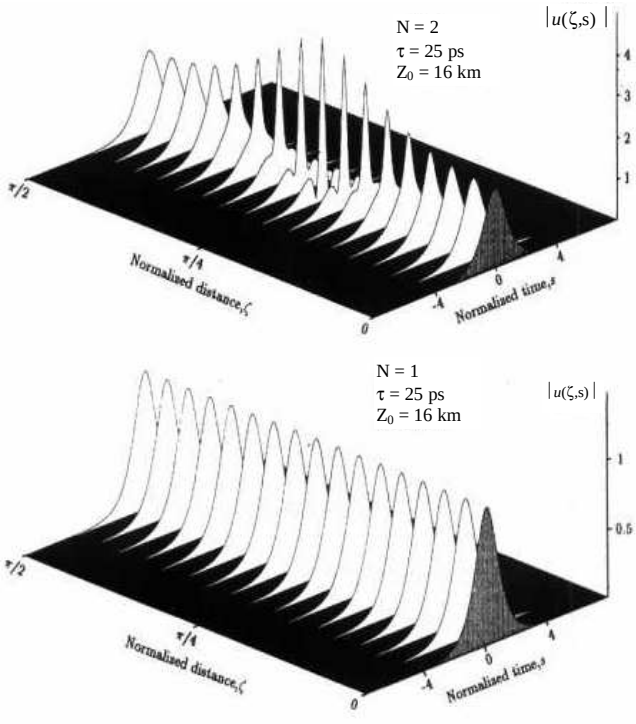

Fig. 3. Three dimensional graphs of first and second order solitons over one period (Γ_l=0).

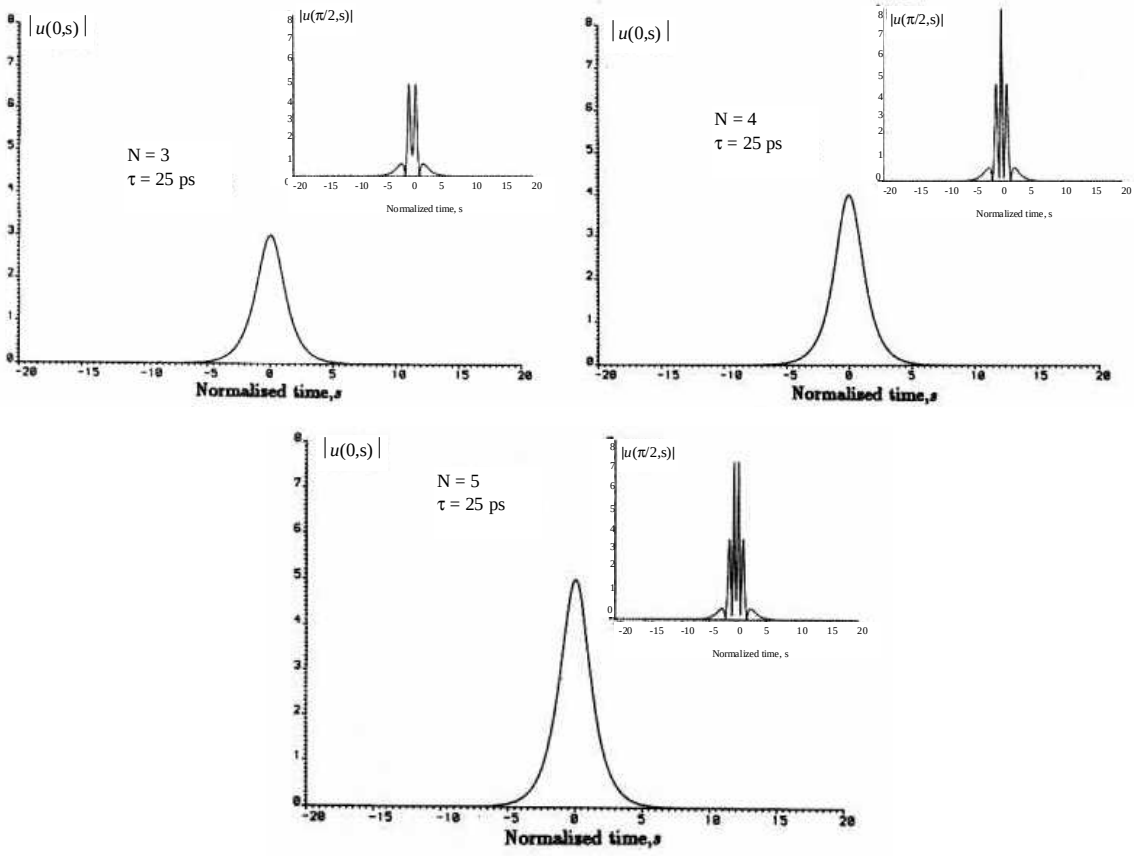

Fig. 4. Higher-order solitons at half period (Γ_l =0).

As it can be seen from Fig. 5, they all develop peaks at the half period and reexpand to the original pulse at the full period. It should be noted that the evolution of all higher-order solitons within the period is symmetrical around $\zeta = \pi/4$. Al higher-order solitons can be viewed as the nonlinear superposition of the fundamental first order solitons. For example, the second order soliton shown in Fig. 2 is the nonlinear superposition of two fundamental solitons. Only higher-order solitons can be used to compress the initial pulse duration. The compression ratio increases as the soliton number increases. The point where the optimum compression of the pulse takes place moves toward the input end of the fiber as the solution number is increased. This movement can be seen from the graphs given in Fig. 3 and 5. This compression technique was first used experimentally by Mollenauer and his co-workers [24] who obtained a pulse compression factor of 22. Of course, one should remember that the peak power required producing higher-order solitons increase as the soliton number is increased. Therefore, the peak power required for higher-order solitons except for the first and the second order could not be within the capacity of the semiconductor lasers.

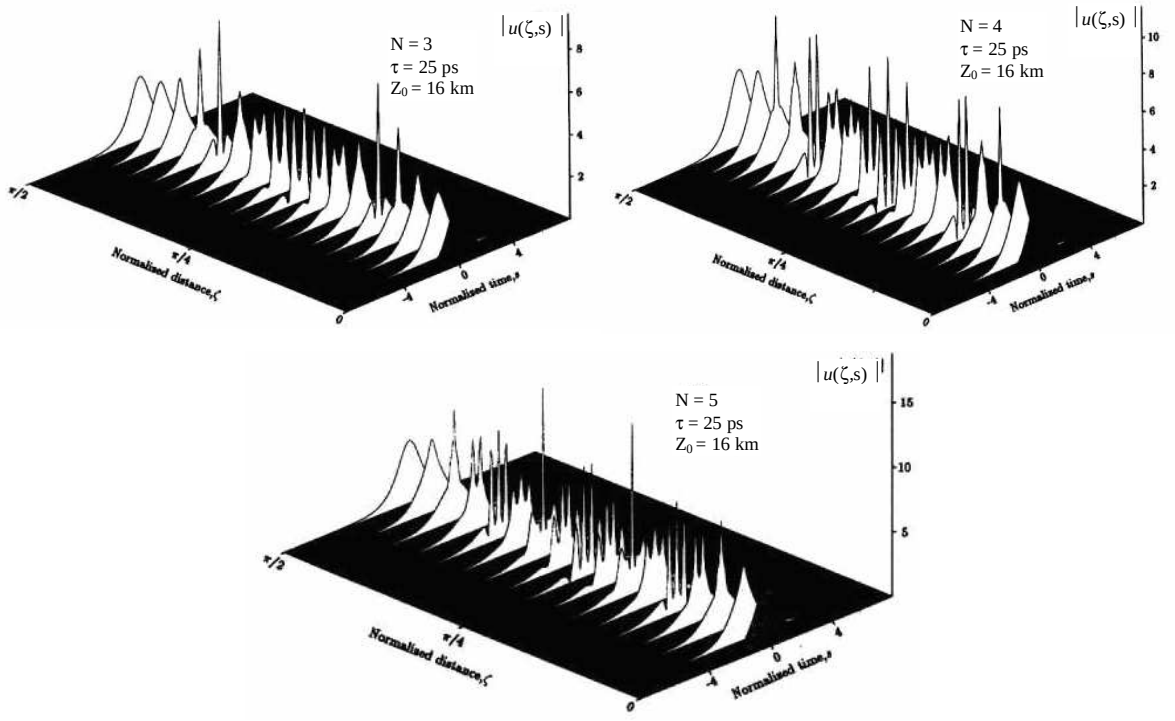

Fig. 5. Three dimensional graphs of higher - order solitons (N=3, 4, 5) over one period (Γ_f=0).

In order to see how the spectrum of the solitons evolves during the propagation in the optical fiber, the spectrum of the pulses are calculated by taking the Fourier transform of the pulses. The three dimensional graphs given in Fig. 6 represent the evolution of the spectrum of the solitons up to the fifth order. As in the temporal evolution, the spectrum of the first order soliton keeps its initial shape throughout the propagation. The spectra of all higher-order solitons are periodic and the initial spectra are restored at the end of the period. Fig. 6 indicates that the higher-order solitons generate more and more peaks both temporally and spectrally. The initial spectra of pulses also broaden due to temporal compression throughout the propagation. The spectral evolution of the higher-order solitons is symmetrical around $\zeta=\pi/4$ as in the temporal evolution picture. Using their pulse compression ability can use higher-order solitons to compensate the broadening effect of the loss. Hasegawa and Kodama [23] has shown theoretically a bit-rate of 1 Tbits/s over 30 km by using the pulse compression ability of the second order soliton. Therefore, only the first and second order solitons are considered in the next sections.

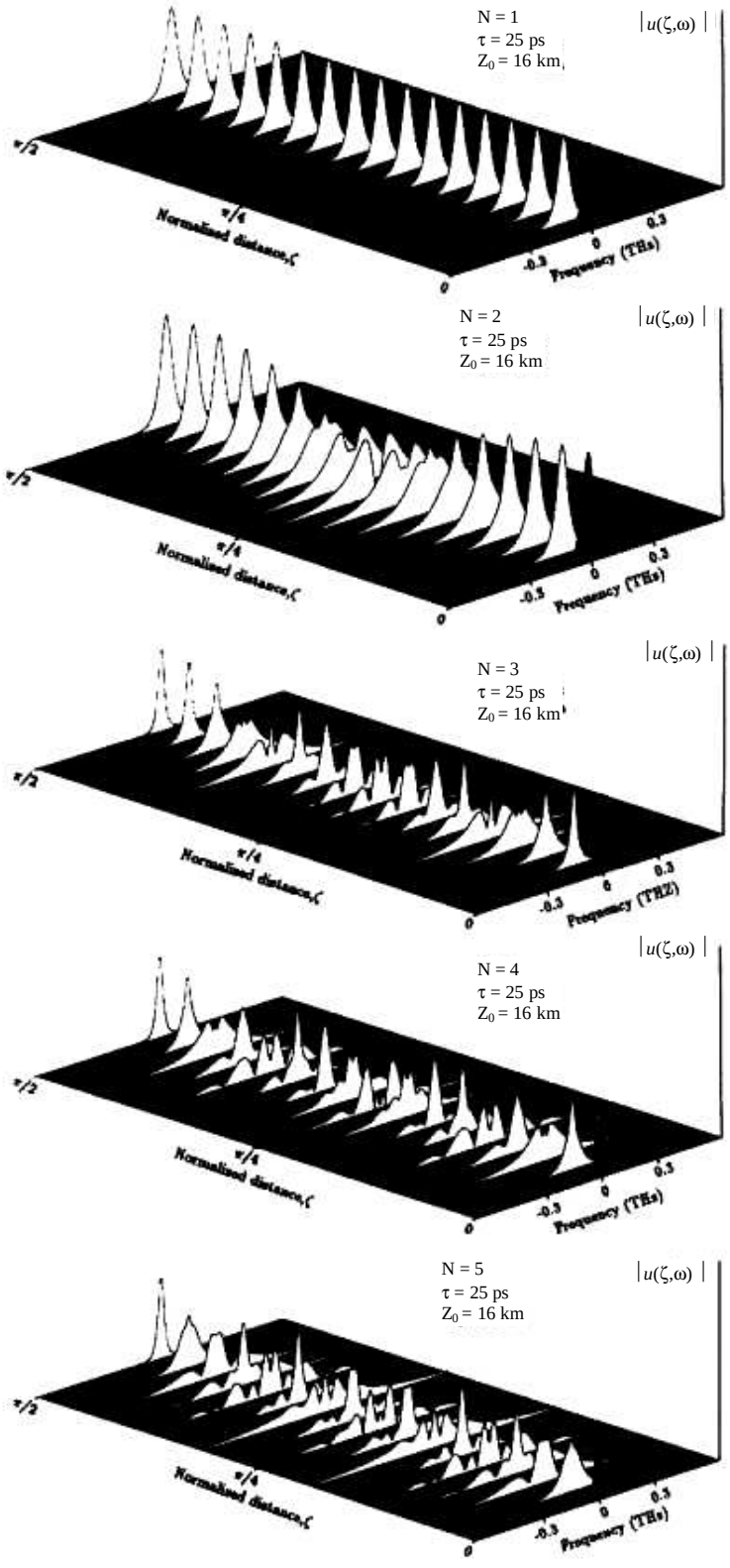

Fig. 6. Three dimensional spectra of solitons (N=1, 2, 3, 4, 5) over one period (Γ_l =0).

4.2 Effect of loss on soliton propagation

In order to see the effect of loss on solitons, the propagation of the first and the second order soliton is simulated for a distance of 69 km with a loss of 0.35 dB/km. For the pulse width of 25 ps, the coefficient (Γ_l) of the loss term in eq. (5) has a value of 0.4. A condition for the perturbation analysis to be valid is given as $\Gamma_l \zeta < 1$ in [25]. Since ζ is 6.8 in the computer simulation the condition is not satisfied. According to this condition, the perturbation analysis is valid up to a distance of $\zeta < 1/\Gamma_l$, which is 2.5. One should remember that the perturbation analysis of the solitons in the presence of the loss is only valid for the first order soliton.

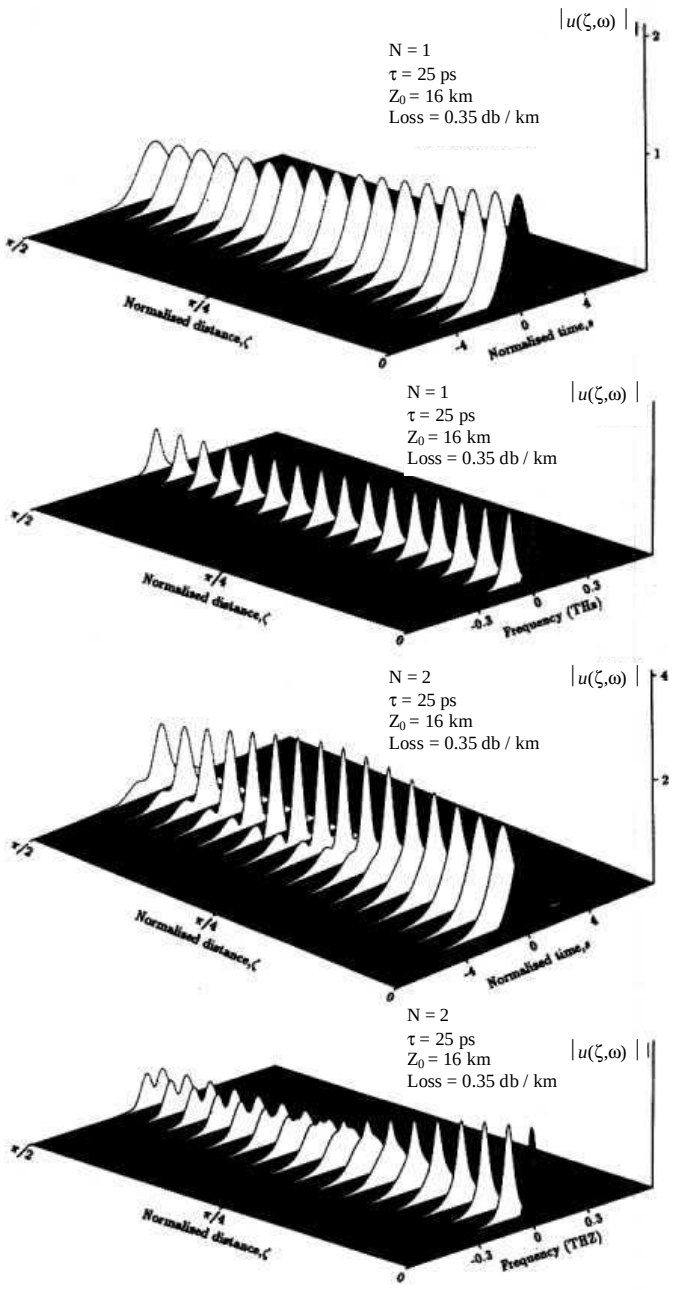

Fig. 7. Temporal and spectral evolution of first and second order solitons in the presence of loss.

Fig. 7 shows the evolution of the first and second order soliton in the presence of loss. The evolution of the pulse spectrum is also shown in Fig. 7. In this figure the amplitude of the first order soliton starts to decrease due to the effect of loss and the width of the pulse is not maintained during the propagation. The width of the first order soliton increases in direct proportion with the loss. The second order soliton in Fig. 7 still initially compresses, but it does not reexpand to the initial pulse shape at the end of the period. The same observation is also true for the evolution of the pulse spectra given in Fig. 7. The effect of the loss on solitons can be easily understood from the soliton period and the fundamental power given by eq. (9) and (10), respectively. The loss causes the fundamental power to decrease and since the fundamental power is inversely proportional to the soliton period, the period increases to compensate the decrease of the power. This means that the soliton period changes with the loss. The increase in the soliton period is only possible if the pulse width increases as well. Therefore, both the soliton period and the pulse width adjust to the decrease in the power. The change in the pulse width also results in rescaling of Γ_l in the PNLS equation. This rescaling of Γ_l in turn accelerates the increase in the soliton period and the pulse width. So, the first effect of the loss is to modify the period of the second order soliton and the second effect is to broaden the pulses.

$$W_{RMS} = 2\left\{\frac{\int_{-\infty}^{\infty}|u|^2 s^2 ds}{\int_{-\infty}^{\infty}|u|^2 ds} - \frac{\int_{-\infty}^{\infty}|u|^2 s ds}{\int_{-\infty}^{\infty}|u|^2 ds}\right\}^{1/2} \tag{22}$$

In addition to the pulse width ratio, pulse peak, pulse energy and pulse area are also numerically computed. Fig. 8 displays the pulse width ratio of the first order soliton as a function of the propagated distance.

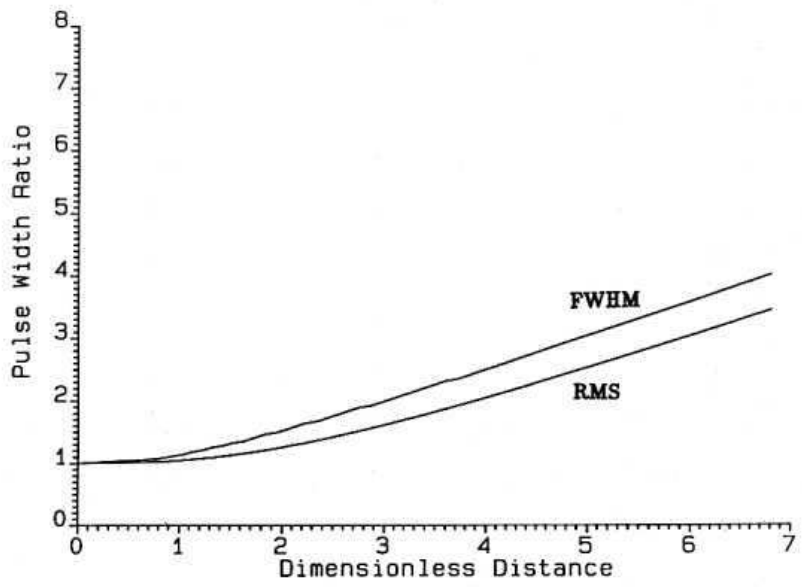

Fig. 8. Pulse width ratio (FWHM and RMS) of first order soliton versus dimensionless distance for τ = 25 ps and γ_{dB} = 0.35 dB/km (1 unit ≡10.2 km).

The width of the pulse stays the same up to a distance of ζ = 0.8 and then starts to broaden as distance increases. This broadening of pulse is almost linear as in the case of linear dispersion. At ζ =6.8, the first order soliton gives pulse width ratios of 4 and 3.4 for FWHM and RMS widths, respectively. For the same distance, the linear dispersion gives a pulse width ratio of the first order

soliton. For the same distance of propagation, the bit-rate can be increased compared to the linear transmission if the first order soliton be used in the system. The reason why the soliton increases the bit-rate can be explained as follows. The pulse broadens directly with dispersion in the linear system whereas it broadens with the loss in the nonlinear system. But, the amount of broadening in the nonlinear system caused by the loss is less than in the linear case because the fiber nonlinearity always tends to compensate the pulse broadening. Of course, the amount of compensation depends on the power level and the pulse width of the soliton. Although the width ratio based on the RMS pulse width gives a smaller value for the first order solution, RMS width does not truly represent the pulse width because it gives undue weight to the pulse spreading at large distances [26]. The width ration based on the RMS width is plotted to show the difference between the two measures of the pulse width. Fig. 9 depicts the variation of the pulse energy, the pulse area and the pulse peak of the first order soliton with the propagation distance. The graphs of these quantities indicate that they decrease exponentially with distance, which was predicted by the perturbation analysis [25]. For short distances $\zeta < 1$, the energy, the area and the pulse peak reduce as $\exp(-2\Gamma_1\zeta)$, $\exp(-\Gamma_1\zeta)$ and $\exp(-\Gamma_1\zeta)$, respectively, At large distances, decrease in these quantities does not follow the exponential decrease given above. This is due to the fact that the perturbation analysis is not valid for large distances where Γ_1 gets bigger and bigger as a result of increase in the pulse width.

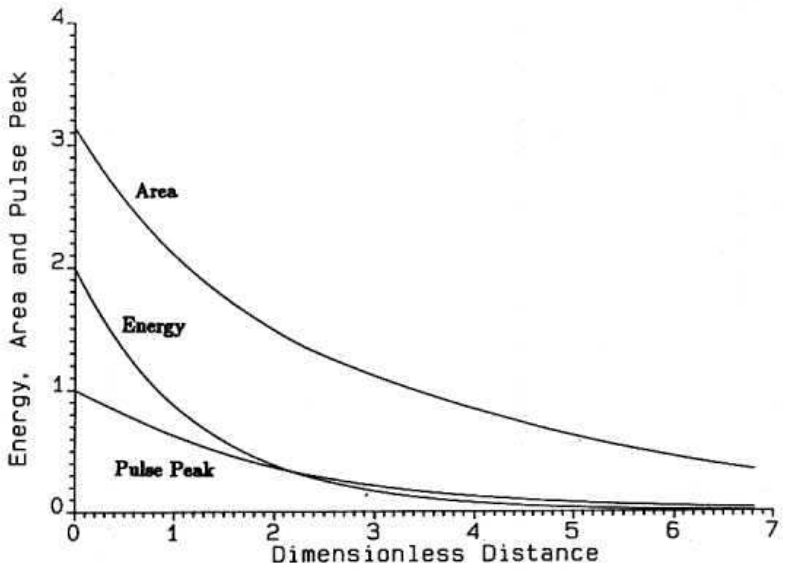

Fig. 9. Energy, area and pulse peak of first order soliton versus dimensionless distance for τ =25 ps and γ_{dB} =0.35 dB/km (1 unit ≡10.2 km).

The pulse width ratio of the second order soliton is presented in Fig. 10 as function of distance for two measures of the pulse width. The following observations are based on the FWHM measure. First, the second order soliton compresses to a minimum pulse width at ζ=0.85 with a compression factor of 2.5 instead of $\zeta = \pi/4$ and a compression factor of 4 as in the case of lossless propagation. Secondly, it recovers its initial pulse duration at ζ=2.1 compared to $\pi/2$. These are the immediate effects of the loss on the second order soliton. Due to large Γ_1, the second order soliton having an initial pulse duration of 25 ps does not show a periodic behavior with different periods at the end of each period. After reexpanding to its initial pulse width, the width of the second order soliton continuously increases with the distance.

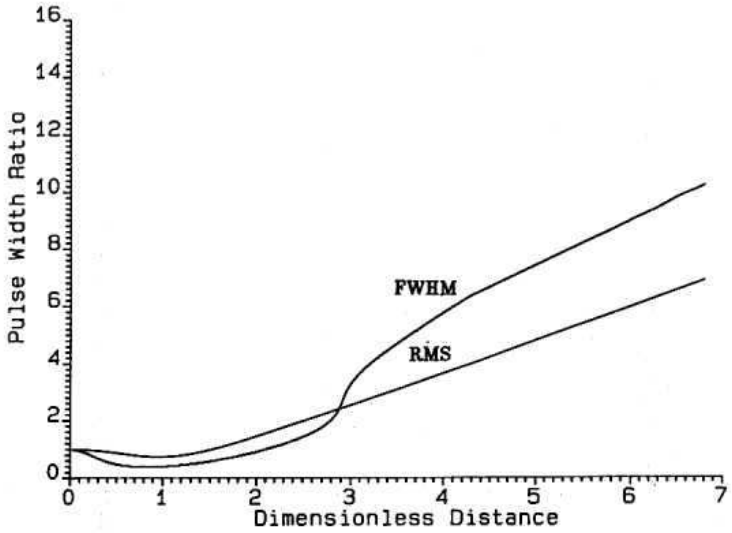

Fig. 10. Pulse width ratio (FWHM and RMS) of second order soliton versus dimensionless distance for τ=25 ps and γ_{dB} =0.35 dB/km (1 unit ≡10.2 km).

The increase in the pulse width is nearly linear after a distance of ζ =3. At ζ =3, the pulse width ratio is 3 compared to 2.8 of the linear case. Whereas the pulse width ratio is 10 at ζ=6.8 and the linear dispersion gives a value of 6 at the same distance. This indicates that the second order soliton enters the linear regime after ζ=3 at which the pulse broadening is mainly due to dispersion. As compared to the first order soliton, the second order soliton broadens more at ζ=6.8 due to the effect of the loss. Hence, the second order soliton cannot be used directly in an optical communication system. But, the initial compression of the second order soliton can be used to compensate for the pulse broadening in the first order soliton. That is, a nonlinear pulse can be generated by launching an initial pulse, which has amplitude N>1 to tailor the initial pulse compression. Fig. 11 represents the variation of the energy, the area and the pulse peak for the second order soliton as a function of the distance.

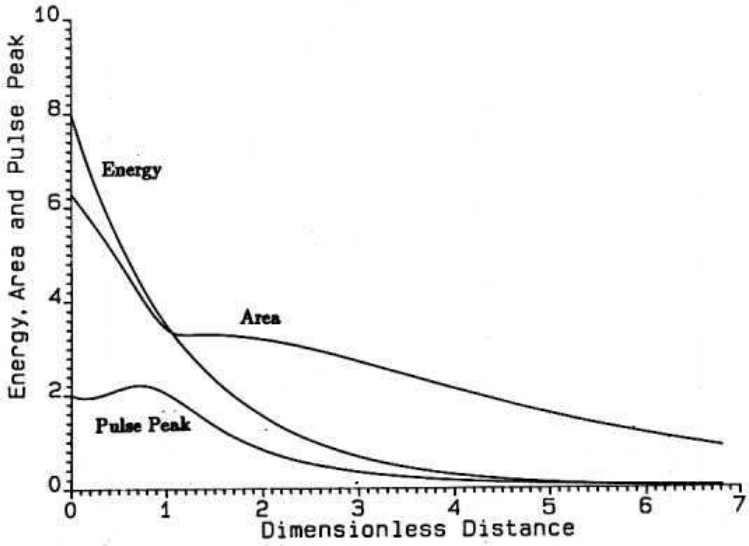

Fig. 11 Energy, area and pulse peak of second order soliton versus dimensionless distance for τ = 25 ps and γ_{dB} =0.35 dB/km (1 unit ≡10.2 km).

The curves for the area and the pulse peak are completely different than for the first order soliton. This is due to the fact that the second order soliton does not preserve its initial pulse shape during the propagation in the optical fiber. The variations in the pulse peak and the pulse area of the second order soliton reflect its shape changing character. The pulse energy decreases exponentially again as in Fig. 9. The variation in the energy, which is related to the total number of photons in the pulse, is independent of the pulse shape and its decrease is only due to the loss of the optical fiber. Hence, the variation of the energy is the same for all solitons. The pulse peak attains its maximum value at the same distance of ζ =0.85 where the pulse width compresses to its minimum value. After ζ =0.85 the amplitude starts to decrease. The same behavior can be seen from Fig. 11 for the pulse area. It should be noted that these results are correct for the pulse having an initial width of 25 ps in which the loss coefficient Γ_l is high. Since Γ_l is a function of pulse duration, the different pulse duration will scale Γ_l differently. Hence, the results will be different form the results given here. In the next section, the propagation of the first and second order solitons are considered with different pulse widths.

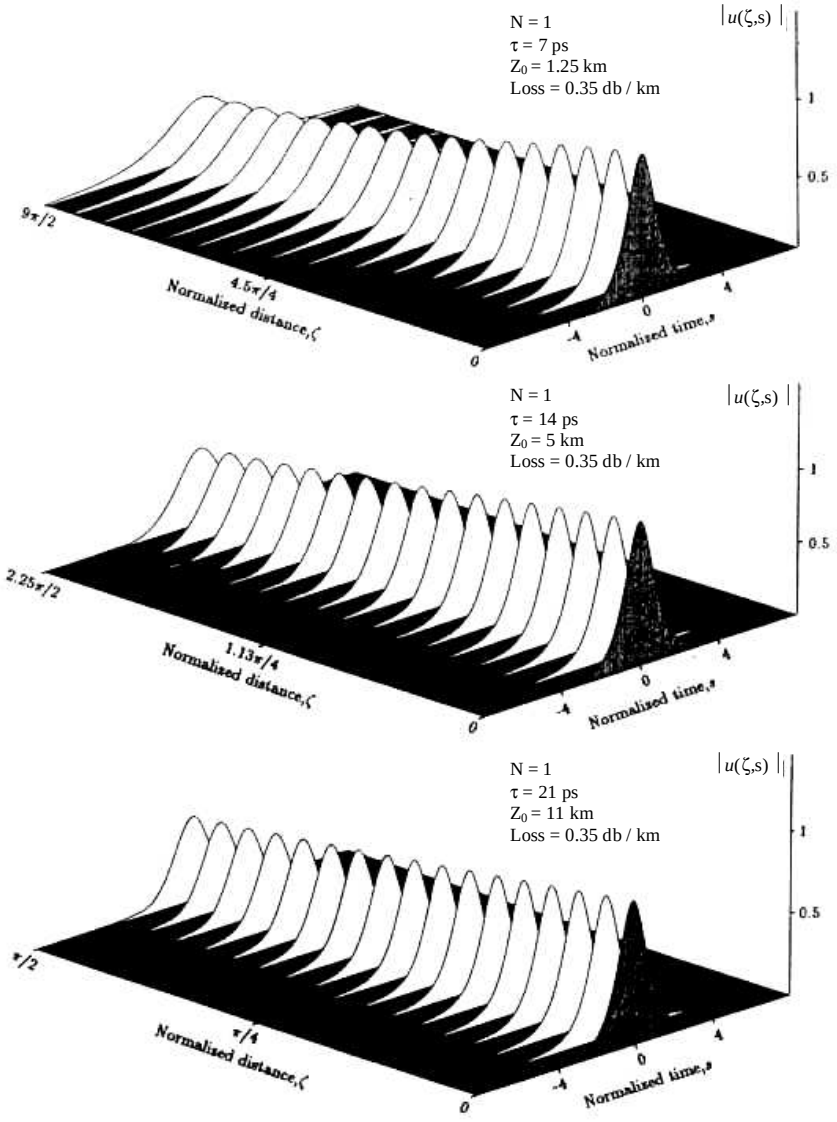

Fig. 12. Three dimensional graphs of first order solitons for τ =21, 14 and 7 ps and γ_{dB}=0.35 dB/km.

4.3 Effect of pulse width on soliton propagation

The propagation of solitons having initial pulse widths of 7 ps, 14 ps and 21 ps is considered in this section. The soliton periods are 1.25 km, 5 km and 11 km, respectively. Since the coefficient of the loss term scales with the pulse width, the propagation of the solitons with the different pulse widths is actually equivalent to the propagation of the soliton having the same initial pulse width, but with loss rates of 0.032, 0.128 and 0.288, respectively.

Fig. 12 shows the three dimensional graphs of the first order soliton with the three different pulse widths. The solitons with 7 ps and 14 ps pulse widths are propagated up to the period of the soliton of width 21 ps. The soliton having 21 ps initial pulse width is propagated one period. The graphs given in Fig. 12 clearly show that the first order soliton with the initial width of 7 ps broadens more at the end of the propagation distance than the 14 ps and 21 ps solitons. In order to see the effect of the loss, these solitons are further propagated up to a distance of 31 km. The pulse width ratios (FWHM) of the first order soliton corresponding to the above pulse widths are plotted in Fig. 13.

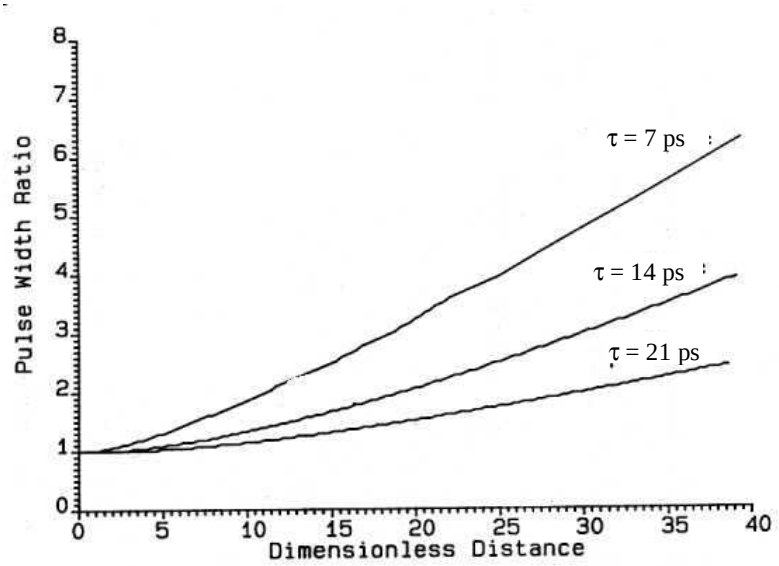

Fig. 13. Pulse width ratio of first order solitons versus dimensionless distance for τ = 21, 14 and 7 ps and γ_{dB}=0.35 dB/km (1 unit ≡ 0.8 km).

One of the immediate observations that can be made from Fig. 13 is that the shorter pulse spreads more than the longer pulse over the same distance which is the same as occurs in the case of the linear dispersion, but the magnitude of the spread is less. The linear dispersion gives pulse width rations of 35, 8.8 and 4 corresponding to 7, 14 and 21 ps pulses whereas the pulse width ratios of the first order soliton for the same pulse widths are 6.2, 4 and 2.4 ps at a distance of 31 km. Although the pulse width ratios of the linear dispersion for 14 and 21 ps pulses are two orders of magnitude bigger than the corresponding soliton broadening, this factor is 5.5 for 7 ps pulse. This is due to the fact that broader pulses which have larger loss coefficients than the 7 ps pulse enter the linear regime earlier. That is, the effect of loss on the 7 ps soliton is less pronounced. Hence, in contrast to the linear dispersion, the first order soliton with a shorter pulse width is advantageous to use in an optical fiber communication system. But this does not mean that the first order soliton with a shorter pulse duration and, correspondingly, smaller loss coefficient broadens less compared to the first order soliton with a longer pulse duration. Fig. 13 shows that the pulse width ratio at a certain distance increases if the initial pulse width is decreased. On should expect that the first order 7 ps soliton should have a smaller pulse width ratio due to smaller loss coefficient. But the graphs given in Fig. 13 show that the opposite is the case. This can be explained with the help of the loss coefficient and the transformation used for the dimensionless distance given by eq. (3). For a fixed value of the pulse duration and optical loss, the loss coefficient increases if the dispersion is decreased since the loss coefficient is

inversely proportional to the dispersion. The decrease of the dispersion will result in a decrease in the dimensionless coordinate ζ for a fixed value of the real distance. This means that the first order soliton with a larger initial pulse width and a large loss coefficient is propagating a shorter distance in dimensionless units than the first order soliton with a shorter initial pulse width. The first order solitons shown in Fig. 13 are propagated for distances of 40, 10 and 4.4 in dimensionless units, for 7ps, 14 ps and 21 ps pulses, respectively. Hence, the broadening of the first order soliton with larger initial pulse width will be less due to effect of the same loss rate for a fixed value of the real distance.

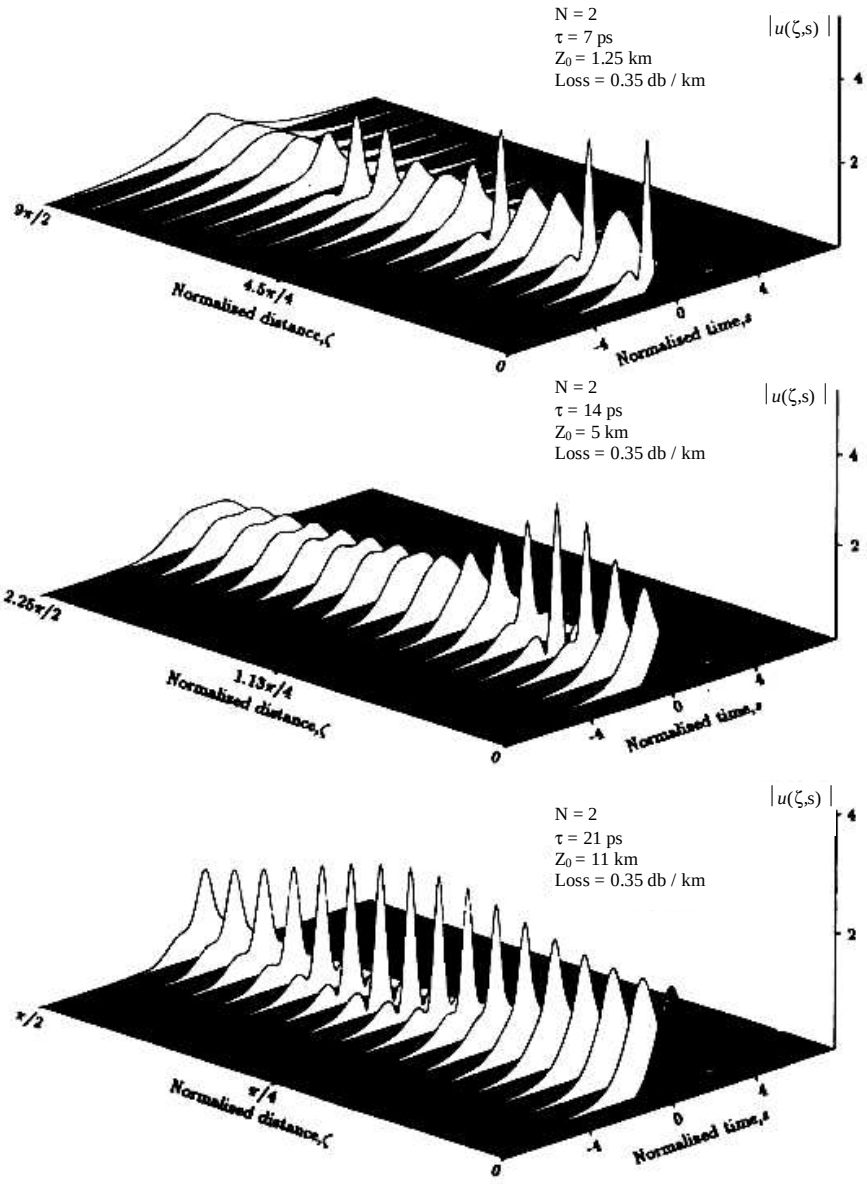

Fig. 14. Three dimensional graphs of second order solitons for τ = 21, 14 and 7 ps and γ_{dB}=0.35 dB/km.

Fig. 14 shows three-dimensional graphs of the second order soliton with different pulse widths. The second order 21 ps soliton is propagated one period, while the 7 ps and 14 ps solitons are

propagated 9 and 2.25 times of their respective periods, as it is known that the loss will modify the period of the soliton. The amount of variation in the soliton period depends on the value of the loss coefficient. The variation of the soliton period can be easily seen from Fig. 14 for the second order 7 ps soliton. Due to the larger loss coefficient of the second order 14 ps soliton, this variation in the soliton period is less pronounced, although it is propagated for 2.25 times its original period. Hence, the other periods cannot be seen in Fig. 14. The second order 21 ps soliton in Fig. 14 is still reexpanding to its initial shape, which will happen at a longer distance due to its large loss coefficient.

The pulse width ratios of the various second order solitons in Fig. 15. It can be seen from Fig. 15 that the period of the 7 ps soliton gets progressively larger and eventually the second order soliton will enter the linear regime where there is no further periodicity in the pulse shape. The second order 14 ps soliton is still compressing after its first period. whereas the second order 21 ps soliton starts to broaden after its first period and its second period will occur at a longer distance. The extended periods of the 7 ps, 14 ps and 21 ps solitons are 3.8 km, 7.6 km and 15.2 km, respectively. Since the variation in the period is different for the three pulse widths due to different loss coefficients, entry into the linear regime will occur at different distances. For the second order 7 ps soliton this will occur earlier because it propagates further in units of the dimensionless coordinate ζ. But if the loss coefficient Γ_l is too big, the period of the soliton will be too long. Hence, the second order soliton with the longer initial pulse duration will enter the linear regime after its first compression without showing any second period. Once the solitons enter the linear regime, the pulse shows no structure and its shape will be different from the initial shape. The pulse width ratios of the second order solitons at ζ =10 can be seen from Fig. 15 to be 10.8, 1.7 and 5.6 for the 7 ps, 14 ps and 21 ps pulses. Among these second order solitons, the 14 ps pulse is interesting because it shows how the second order soliton improves the bit rate compared to the first order soliton with the same pulse with the same distance. The first order soliton gives a pulse width ration of 4 which is three times bigger than the pulse width ratio of the second order soliton. This is due to the fact that the second order soliton is still compressing at ζ =10 while the first order soliton is continuously broadening at ζ=10.

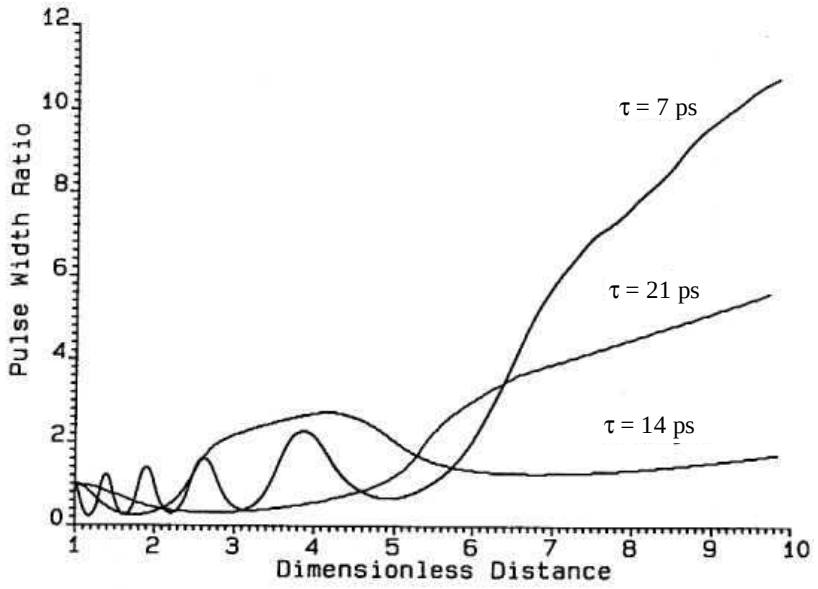

Fig. 15. Pulse width ratio of second order solitons versus dimensionless distance for τ =21, 14 and 7 ps and γ_{dB}=0.35 dB/km (1 unit ≡3.2 km).

The second order 7ps and 14 ps solitons give larger pulse width ratios than the first order soliton with the same pulse widths at ζ=10. This is because these second order solitons are in the reexpanding stage where the pulse width ratios are bigger compared to the pulse width ratios in the

compressed stage. Hence, the pulse width ratios of these second order solitons should be compared to the first order soliton during the compression stage. For example, the second order 7 ps soliton gives a pulse width ratio of 2.8 at the same distance. So, improvement in the pulse width ratio depends on whether the second order soliton is its compression stage. Hence, the bit-rate of a soliton-based communication system can in principle be increased by using second order solitons instead of first order solitons, if the initial pulse parameters of the second order soliton is chosen properly. The compression factors obtained with different pulse widths are 4, 3.3 and 2.5 for 7ps, 14 ps and 21 ps pulses, respectively. The factors indicate that the smaller loss coefficient will give a larger compression factor. This is expected because if the perturbation in the PNLS equation is reduced, the compression factors approach the lossless case. In the lossless case, the second order soliton gives a compression factor of 4 which is same compression factor obtained for the second order 7 ps soliton. So, shorter pulses should be used for obtaining larger compression factors.

5. Conclusions

All the aspects of solitons and soliton propagation in optical fibers have been widely investigated for the purpose of implementing high bit-rate and long-distance optical fiber communication systems using solitons generated by semiconductor lasers.

The nonlinear Schrödinger equation including the loss term is numerically solved in the picosecond domain by split-step Fourier transform technique for the case of soliton propagation at 1.55 μm where the optical loss is minimum. Two important quantities, the soliton period and the fundamental power, which interlink the initial pulse parameters and dispersion of the optical fiber, are also derived from the normalization equations for the nonlinear Schrödinger equation. The results obtained for solitons up to fifth order in the lossless case demonstrate some of the properties of solitons such as the shape-preserving property of the first order soliton and periodicity, splitting and compression properties of higher-order solitons. Since higher-order solitons require more peak power, the propagation of only the first and second order solitons are considered under the effect of optical loss. It has been found that the optical loss broadens the pulse width of solitons and increases the soliton period. However, this broadening in the pulse width is directly proportional to the optical loss unlike the broadening effect of dispersion. Numerical calculations for an initial pulse width of 25 ps show that the use of the first order soliton in optical communication systems can improve the bit-rate compared to the linear case even if no precaution is taken against the pulse broadening effect of fiber attenuation. For the same initial pulse width of 25 ps and a propagation distance of 69 km, a pulse broadening ratio of 4 for the first order soliton has been obtained compared to the pulse broadening ratio of 6 for the linear dispersion.

The propagation of first order solitons with different pulse widths indicates that shorter initial pulses spread more than longer ones although the loss coefficient in the PNLS equation is smaller. This seems contradictory because when the perturbation in the PNLS equation is decreased, one would expect to approach the solution in the lossless case; hence the broadening of the first order soliton should be decreasing. But, the effect of the loss is to put the solitons into the linear regime where they propagate under the effect of the dispersion only. Linear dispersion theory gives larger pulse width ratios for shorter initial pulse duration. Therefore, the numerical results are not contradictory to that predicted by the linear dispersion case.

Numerical results obtained for the propagation of the second order soliton with different initial pulse widths show that the bit-rate of a soliton-based communication system can be further improved over the first order soliton system if the compression property of the second order system is utilized. The improvement in the bit-rate over the same distance of propagation as the first order soliton, depends on the initial pulse width. That is, the initial pulse width of the second order system should be adjusted in such a way that its compression stage should occur at the same propagation distance of the first order soliton with the same initial pulse width. A pulse compression factor of 2.5 for standard parameters has been obtained from the computer results for the second order soliton. This pulse compression will take place at a distance of 8.7 km compared to $Z_o/2$ for the lossless case where the soliton period Zo is 16 km for an initial pulse width of 25 ps. The computer simulation of the second order soliton propagation depicts that pulse compression is possible even in the presence of

loss. The amount of compression depends on the initial pulse width of the soliton. Although shorter initial pulse widths give larger compression factors than longer ones, the fundamental power increases if pulse width is decreased. Therefore, the initial pulse width of the soliton should be chosen appropriately to obtain a compromise between the fundamental power and the amount of compression. In conclusion, the solitons can improve the bit-rate of optical communication systems and they can be generated from low power pulses and in large soliton period regime even in the presence of optical loss if the necessary peak power could be obtained from semiconductor lasers generating picosecond duration pulses.

The problems related to the self - modulation during the longitudinal and transversal propagation of the optical field in optical fibers have been later developed in [27 - 29]. In [29] have been obtained analytical solutions regarding the compression of the optical solitons at the level of small and large signal. The obtained results are in a quite good agreement with the results obtained by us. In the paper [30] a more complete model was achieved, which characterizes the compression of the "dark" type optical solitons. In [31] is evidenced the compression process of the optical solitons resulting from the compensation of the third order negative dispersion and from the Raman self - scattering.

Finally, we mention that the problems analyzed by us have determined later the development of models related to the transversal and longitudinal instabilities of the three-dimensional optical solitons [32]. Thus, an important problem has been resolved in [33]: transversally stabilized soliton vortex by solitaire longitudinal waves. As show in the paper [34] the three-dimensional model allows to get interesting correlation between the longitudinal transversal instabilities with applications in the design and sizing of the communication system based on optical fibers.

References

[1] T. Miya, Y. Terunuma, T. Hosaka, T. Miyashita, Electron. Lett. **15**, 106 (1979).
[2] C. Gloge, Appl. Optics **10**, 2442 (1971).
[3] A. W. Snyder, Proc. IEEE **69**, 6 (1981).
[4] W. A. Gambling, H. Matsumara, C. M. Ragdale, Electron. Lett. **15**, 474 (1979).
[5] A. Hasegawa, F. Tappert, Appl. Phys. Lett. **23**, 142 (1973).
[6] A. Hasegawa, F. Tappert, Appl. Phys. Lett. **23**, 171 (1973).
[7] V. E. Zakharov, A. B. Shabat, Sov. Phys. JETP **34**, 62 (1972).
[8] J. Satsuma, N. Yajima, Suppl. Progr. Theor. Phys. **55**, 284 (1974).
[9] D. N. Christodoulides, R. I. Joseph, Opt. Lett. **9**, 408 (1984).
[10] K. J. Blow, N. J. Doran, Phys. Lett. **107A**, 55 (1985).
[11] P. A. Belanger, P. Mathieu, Appl. Opt. **26**, 111 (1987).
[12] L. F. Mollenauer, R. H. Stolen, J. P. Gordon, Phys. Rev. Lett. **45**, 1095 (1980).
[13] L. F. Mollenauer, R. H. Stolen, Fiberoptic Tech. **IV**, 193 (1982).
[14] L. F. Mollenauer, Phil. Trans. Roy. Soc. **A315**, 437 (1985).
[15] R. H. Stolen, C. Lin, Phys. Rev. **A17**, 1448 (1978).
[16] M. S. Ozyazici, Ph. D. Thesis, University of London, 1988.
[17] R. H. Hardin, F. D. Tappert, SIAM **15**, 423 (1973).
[18] D. Yevick, B. Hermansson, Opt. Communic. **47**, 101 (1983).
[19] N. J. Doran, K. J. Blow, IEEE J. Quantum Electron. **QE-19**, 1883 (1983).
[20] J. A. Fleck, J. R. Morris, M. D. Feit, Appl. Phys. **10**, 129 (1976).
[21] M. Lax, J. H. Battch, G. P. Agrawal, J. Appl. Phys. **52**, 109 (1981).
[22] M. Lax, G. P. Agrawal, M. Belic, B. J. Coffey, W. H. Louisell, J. Opt. Soc. Am. **A2**, 731 (1985).
[23] A. Hasegawa, Y. Kodama, Proc. IEEE **69**, 1145 (1981).
[24] L. F. Mollenauer, R. H. Stolen, J. P. Gordon, W. J. Tomlinson, Opt. Lett. **8**, 289 (1983).
[25] K. J. Blow, N. J. Doran, Opt. Commun. **42**, 403 (1982).
[26] K. J. Blow, D. Wood, Opt. Commun. **58**, 349 (1986).
[27] N. N. Akhmediev, J. M. Soto-Crespo, Dynamics of soliton like pulse propagation in birefringent optical fibers, Phys. Rev. E, **49**(6), 5742 (1944).

[28] N. N. Akhmediev, E. A. Ostrovskaya, Counxter-balance of linear and nonlinear optical activity for soliton-like pulses, Opt. Appl. **XXVI**(4), 267 (1996).
[29] E. Fazio, V. Babin, M. Bertolotti, V. I. Vlad, Soliton like propagation in photorefractive crystals with large optical activity and absorption, Phys. Rev. E, Nr. 66, 016605 (2002).
[30] Wen-hua Cao, You-wei Zhang, The effect of pulse walkoff on the compression of light optical pulses by dark solitons, Opt. Comm. **128**, 23 (1966).
[31] Kam-tai Chan, Wen-hua Cao, Improved soliton effect pulse compression by combined action of negative third-order dispersion and Raman self-scattering in optical fibersm J. Opt. Soc. Am B, **15** (9), 2371 (1998).
[32] T. J. Alexender, A. V. Buryak, Y. S. Kivshar, Stabilization of dark and vortex parametric spatial solitons, Opt. Lett. **23**(9), 670(1998).
[33] A. Picozzi, Three-dimensional hybrid solitary wave: Transverse vortex solitons stabilizated by longitudinal parametric solitary waves, Phys. Rev. E. **64**, 016614-1 (2001).
[34] V. I. Vlad, V. Babin, A. Mocofanescu, Analytical treatment of the three-dimensional model of stimulated Brillouin scattering with axial symmetric pump wave, J. Optoelectron. Adv. Mater. **4**(3), 581 (2002).

Part II. Fiber Bragg grating design for mode-locked hybrid soliton pulse source

1. Introduction

Single mode, narrow linewidth semiconductor lasers are key components in long-haul, high bit-rate fiber optic communication systems. DFB and DBR lasers and some hybrid structures incorporating a Bragg reflector [2,3] are good candidates to be used as a source in these systems. Ultra long distance soliton transmission systems, however, require relatively long pulsewidths and hence a narrow optical bandwidth. One of the most promising hybrid devices for the long distance soliton transmission systems is the Hybrid Soliton Pulse Source demonstrated first by Morton *et al.* [1]. The device is comprised a strained MQW laser, a fiber and a Bragg reflector in a single package. It has been shown that HSPS can be mode-locked over an unusually wide frequency range (2.2-2.8 GHz [1,4]), although the cavity is designed to be operated at the SONET frequency 2.488 GHz. This feature of the HSPS is a result of the novel wavelength self-tuning mechanism employed by the use of the chirped Bragg reflector. Having these specifications, HSPS was used in a soliton transmission experiment at 10 Gb/s over 27000 km [5].

In order to simulate the operation of a device including a fiber Bragg grating, the refractive index variation along the grating must be known. With the help of mathematical models, it is possible to determine the reflection and group delay spectrums as well as the coupling distribution provided by the grating. It is known that the reflection characteristics of Bragg reflectors with a constant pitch (uniform) have many side lobes [6,7,8], depending on the coupling strength. However, for practical applications these side lobes must be eliminated to have a good filter response. For this reason, some chirp must be introduced while writing the Bragg reflector [4,6,7,9] in addition to apodizing the refractive index profile of the grating. Although it is possible to apply many apodization functions to the grating during fabrication [8,10], we assumed that the index profile of the grating is written by a UV Gaussian laser beam and hence the grating is Gaussian apodized. It is known that an apodized grating with a proper amount of chirp results in a single-lobed reflection spectrum together with an almost uniform group delay [7,8]. Therefore, the use of gratings with these specifications in hybrid structures, such as HSPS, may result in a more stable operation of the system [1,4].

In this work, a nonlinear refractive index profile with a different chirp term from those given in [7] and [8] is used. The coupled-mode equations are derived according to this profile. A fiber Bragg grating model is developed from the piecewise-uniform solution of the coupled-mode equations. Although the model described in this work is for the Gaussian apodized and linearly chirped Bragg gratings, it can be used for any refractive index profile. The effects of the index change amplitude, wavelength chirp, grating length and the modulation index on the response of grating are determined. The results are examined according to the criteria for a proper operation of the HSPS [1,4].

2. Theory

The fiber Bragg grating considered in this work is a single mode optical fiber whose core is written by a Gaussian laser beam along $z = -L/2$ to $z = L/2$.

The variation of the perturbated core index can be formulated as

$$n_c(z) = n_{co} + \Delta n_{co}(z)\left[1 + m\cos\left(\frac{2\pi}{\Lambda(z)}z\right)\right] \tag{1}$$

where m is the modulation index (or fringe visibility) of the index change, n_{co} is the refractive index of the unperturbated fiber core (taken as 1.46) and $\Delta n_{co}(z)$ is the slowly varying envelope function of the index perturbation ($\Delta n_{co} << n_{co}$). The z-dependent grating period $\Lambda(z)$ is linearly chirped and is taken as

$$\Lambda(z) = \Lambda_o + \frac{1}{2n_{co}} \frac{d\lambda_o}{dz} z \tag{2}$$

where $\Lambda_o = \lambda_o/2n_{co}$ is the pitch of the unchirped Bragg grating at the operating wavelength λ_o. The derivative of λ_o with respect to z defines the chirp rate C that is usually expressed in nm/cm. A negative chirp rate means that the period of the corrugation decreases as moving along the positive z direction, while the opposite is true for the positive values of the chirp rate. Inserting Equation 2 into Equation 1 and expanding the term inside the cosine parenthesis as a Taylor series, Equation 1 can be rewritten as

$$n_c(z) = n_{co} + \Delta n_{co}(z) \left[1 + m \cos\left(\frac{2\pi}{\Lambda_o} z - \frac{4\pi n_{co}}{\lambda_o^2} C z^2 \right) \right] \tag{3}$$

In this expansion, it is assumed that $Cz << \lambda_o$. Using the nonlinear index profile in this equation, the coupled-mode equations can be derived following a similar procedure as given in [7,11,12]

$$-F' - j\left(\delta + \frac{2\kappa}{m} + \frac{4\pi n_{co}}{\lambda_o^2} C z \right) F = j\kappa R \tag{4}$$

$$R' - j\left(\delta + \frac{2\kappa}{m} + \frac{4\pi n_{co}}{\lambda_o^2} C z \right) R = j\kappa F \tag{5}$$

where F and R the forward- and reverse-propagating fields, δ is the deviation from the real part of the propagation constant ($\delta = \beta - \beta_o$), and κ is the "ac" coupling coefficient. The following assumptions are made while deriving Equations 4 and 5 from Equation 3: $Cz << \lambda_o$ and $\delta << \beta, \beta_o$. The perturbated refractive index profile and hence the coupling coefficient are taken as Gaussian apodized,

$$\kappa(z) = \kappa_p \exp\left[-\frac{1}{2} \left(\frac{z}{L_H} \right)^2 \right] \tag{6}$$

Here L_H is the half-width of the profile (at $1/e$ intensity point) and κ_p is the peak value of the Gaussian variation. If the half-width in this equation is replaced by the full-width at half-maximum (FWHM) of the κ variation $FWHM_\kappa$, it can be rewritten as

$$\kappa(z) = \kappa_p \exp\left(\frac{-4\ln 2}{FWHM_\kappa^2} z^2 \right) \tag{7}$$

Assuming the whole length of the fiber grating is apodized, the $FWHM_\kappa$ can simply be taken as ~$L/3$. The peak value of the κ is related to the averaged dc index variations by

$$\kappa_p = \frac{\pi \Delta n_{co}}{\lambda_o} m \tag{8}$$

The coupled-mode equations (Equations 4 and 5) derived here are similar to those given in [7] where the derivation starts with the index function

$$n_c(z) = n_{co} + \Delta n_{co}(z) \left[1 + m \cos\left(\frac{2\pi}{\Lambda_o} z + \Phi \right) \right] \tag{9}$$

If the second term in the argument of the cosine function in Equation 3 is defined as the chirp parameter,

$$\Phi = -\frac{4\pi n_{co}}{\lambda_o^2} C z^2 \tag{10}$$

then Equations 3 and 9 will be the same. Although a different procedure is followed throughout the derivations, the resultant coupled-mode equations are also similar to those given in [7]. If the term inside the parenthesis in Equations 4 and 5 is called the dc "self-coupling" coefficient, as in [7]

$$\sigma = \delta + \frac{2\kappa}{m} + \frac{4\pi n_{co}}{\lambda_o^2} C z \tag{11}$$

and the last term in this equation is rewritten as $-(1/2)d\Phi/dz$, then the resultant equations will be the same as those given in [7].

The coupled-mode equations are solved using a piecewise-uniform approach. First the equations are solved analytically and then the grating is divided into M sections each having an equal length Δz. Assuming the boundary conditions at $z = L/2$ as $F(L/2) = 1$ and $R(L/2) = 0$, the calculations are carried out back to forth (from $z = L/2$ to $-L/2$), the parameters of each section are calculated and these parameters are put into a 2x2 propagation matrix $\mathbf{T_i}$.

The fields at the i^{th} section can be calculated from the known fields of the previous section such that

$$\begin{bmatrix} F_i \\ R_i \end{bmatrix} = \mathbf{T_i} \begin{bmatrix} F_{i-1} \\ R_{i-1} \end{bmatrix} \tag{12}$$

The propagation matrix for the i^{th} mode can be written as

$$\mathbf{T_i} = \begin{bmatrix} \cosh(\gamma_i \Delta z) - j\frac{\sigma_i}{\gamma_i}\sinh(\gamma_i \Delta z) & -j\frac{\kappa_i}{\gamma_i}\sinh(\gamma_i \Delta z) \\ j\frac{\kappa_i}{\gamma_i}\sinh(\gamma_i \Delta z) & \cosh(\gamma_i \Delta z) + j\frac{\sigma_i}{\gamma_i}\sinh(\gamma_i \Delta z) \end{bmatrix} \tag{13}$$

where the coupling coefficients are related as

$$\gamma_i^2 = \kappa_i^2 - \sigma_i^2 \tag{14}$$

Note that the values of κ_i, σ_i and hence γ_i are different for each section and must be calculated individually before putting into the propagation matrix.

Once all of the matrices for the individual sections are known, the amplitudes at $z = L/2$ can be found from the multiplication of the propagation matrices. After the calculation of the complex fields at the M^{th} section, the field reflection coefficient of the Bragg grating can be calculated from

$$\rho = \frac{R_M}{F_M} \tag{15}$$

After the calculation of the reflection coefficient, the group delay τ_g can be determined from the phase of the reflection coefficient θ_ρ by

$$\tau_g = \frac{d\theta_\rho}{d\omega} \cong -\frac{\lambda^2}{2\pi c}\,\frac{\Delta\theta_\rho}{\Delta\lambda} \tag{16}$$

where ω is the angular frequency, c is the speed of light in vacuum, and $\Delta\theta_\rho$ and $\Delta\lambda$ are very small changes in the phase of reflection coefficient and wavelength, respectively.

The number of sections needed for the calculations is determined by the required accuracy. For most cases, M≅100 is sufficient [7]. M may not be arbitrarily large, since the approximations that lead to the coupled-mode equations are not valid when a grating section is only a few grating periods long. Thus, we require $\Delta z >> \Lambda$ which means that (since $\Delta z = L/M$, $\Lambda = \lambda_o/2n_{co}$)

$$M << \frac{2n_{co}\,L}{\lambda_o} \tag{17}$$

If "<<" is approximated by 100 times, and n_{co} = 1.46 and λ_o = 1.55 μm, this inequality can be rewritten as M < 188 L, where L is in cm. This makes M < 752 for a 4 cm grating.

3. Results

A computer program that calculates the response of the fiber Bragg grating (reflectivity and group delay) at a wavelength range near the Bragg wavelength λ_o is developed. A single mode fiber Bragg grating operating at 1.55 μm is considered in this model. The results are presented in Figs. 1 to 7. The peak reflectivity of the grating is taken as 0.5 [4] in order to make a comparison between the results. The value of κ_p and hence Δn_{co} is calculated by the program according to 0.5 peak reflectivity. The only exception is made for Fig. 2 for which the effects of the index change amplitude is investigated. Similarly, the modulation index is taken as 1 for all results except those given in Fig. 6 for which the effects of the modulation index on the response of the grating are investigated.

The reflection spectrum, its phase and the group delay characteristics of a linearly chirped (-2 Å/cm) grating are given in Fig. 1, where κ_p is calculated by the program as 1.82 (1/cm). The reflection spectrum is asymmetric and its peak is shifted from the design wavelength 1.55 μm to 1550.145 nm. This behavior is because of the chirping and the nonzero average refractive index (as a result of Gaussian apodization).

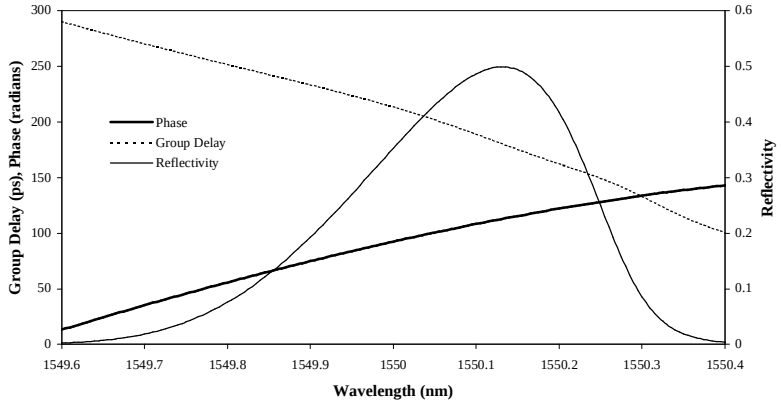

Fig. 1. Reflectivity and group delay spectrums for a Gaussian apodized, linearly chirped grating with a peak reflectivity of 0.5 and C = -0.2 nm/cm.

The effect of the index change amplitude (related to κ_p by Equation 8) on the reflection spectrum of a Gaussian apodized grating is given in Fig. 2(a). The grating has uniform pitch

(unchirped) and is 1 cm long. As it can be seen from the figure, the peak of the reflectivity and its FWHM are higher for stronger gratings, as expected [7,9]. It is possible to make strong gratings by choosing κ_p greater than ~9 (1/cm), with fully reflective spectrum where light can not penetrate into the whole length of the grating. The reflection spectrum in Fig. 2(a) also shows a prominent side-lobe structure observed at the short wavelength side of the spectrum, for stronger gratings. These lobes are the result of the Fabry-Perot effect employed by the grating edges that behave as partially reflecting mirrors [6,7]. This phenomenon has been explained in detail by the effective medium description in [13]. Since a good reflector must have an almost uniform shape of reflection coefficient, the lower κ_p values are better. It can also be seen from Fig. 2(a) that the wavelength corresponding to the peak of the reflection spectrum shifts towards the longer wavelengths for stronger gratings.

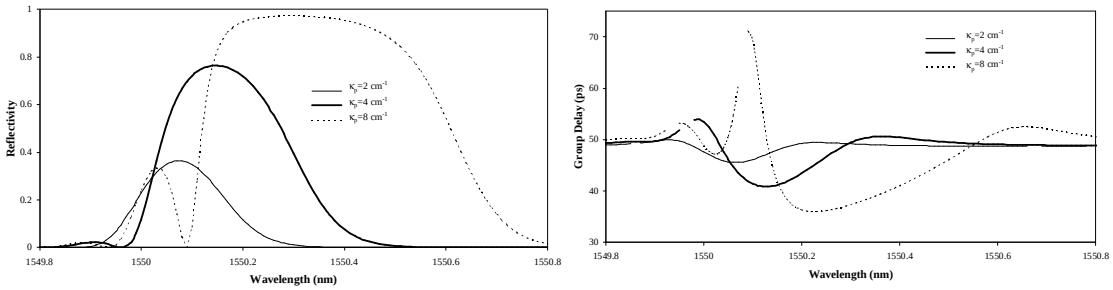

(a) (b)

Fig. 2. (a) Reflectivity and (b) group delay characteristics for Gaussian apodized, unchirped gratings for different κ_p values.

The peaks are located at 1550.08 nm, 1550.16 nm and 1550.29 nm for κ_p = 2, 4 and 8 (1/cm), respectively. This shift is found to be due to the increased nonuniform dc averaged refractive index change [3,6,7]. Since the output of the HSPS is taken from the end of the grating at $z = L/2$, the grating should not be a perfect reflector, instead, the peak reflectivity may lie between 0.5-0.7 range [3,4]. According to these criteria, the κ_p values greater than 4 cm^{-1} and smaller than 3 cm^{-1} are not suitable for HSPS applications since the former results in a very high reflectivity and the latter a very low reflectivity. While determining this range, it is assumed that the other parameters of the grating are kept constant.

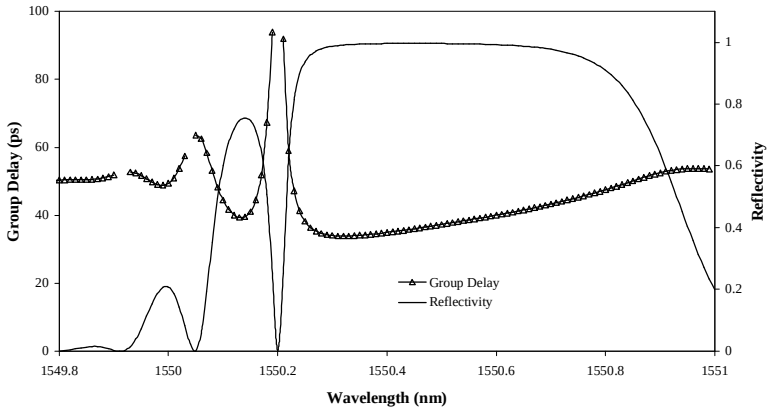

Fig. 3. Reflectivity and group delay characteristics for a Gaussian apodized, unchirped grating with κ_p = 12 cm^{-1}.

The group delay characteristics for different κ_p values are shown in Fig. 2(b). The jump discontinuities in this figure are the result of the side lobes at the reflection spectrum [14,15]. Since

the phase of the reflectivity vanishes (π phase change in the phase of reflection) at the minimums of the spectrum their derivative are discontinuous at these points. Because of these discontinuities, there will also be some unwanted jumps at the dispersion characteristics. For a clearer presentation, the reflection spectrum with more side lobes and the corresponding group delay discontinuities are given in Fig. 3 for κ_p = 12 (1/cm).

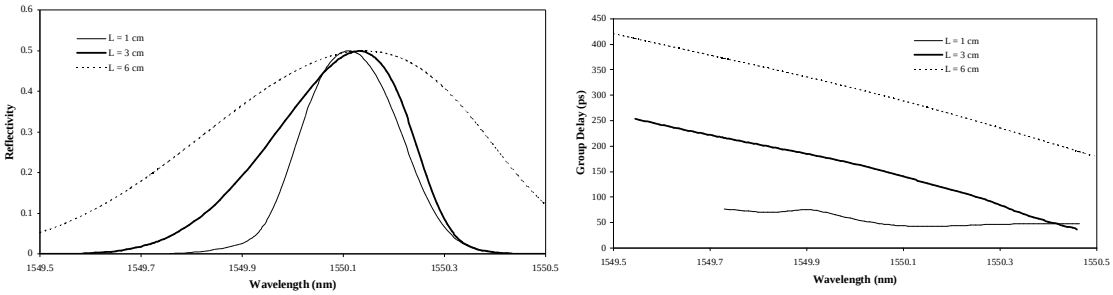

(a) (b)

Fig. 4. (a) Reflectivity and (b) group delay characteristics for the gratings having different lengths. The gratings are Gaussian apodized, linearly chirped (C = -0.2 nm/cm).

Fig. 4(a) shows the change in the reflection spectrum with the grating length. The peak reflectivity is chosen as 0.5 and the κ_p of the grating is adjusted for each grating length to give 0.5 maximum reflectivity. There are no significant side lobes in this figure since the grating is linearly chirped at a rate of –1 Å/cm. As the length of the grating is increased, the FWHM of the reflection spectrum increases as well. The FWHMs of the spectrums are 2.25 Å, 3.1 Å and 6.3 Å for 1 cm, 3 cm and 6 cm long gratings, respectively. Since the wider the FWHM of the reflection spectrum, the better the wavelength self-tuning for mode-locked HSPS [4], it is preferable to have a longer grating. Although it is not noticeable, the peak wavelength of the reflection spectrum shifts towards the longer wavelengths as the length of the grating is increased. The group delay curves for the gratings having different lengths are shown in Fig. 4(b). The group delay curve with respect to the wavelength becomes linear for longer gratings. With the help of this feature, HSPS can be mode-locked for a wider frequency range, since the whole reflection spectrum can be used [4]. Because the group delay curve for the 1 cm long grating is nonlinear, its application to an external cavity system will not produce good results.

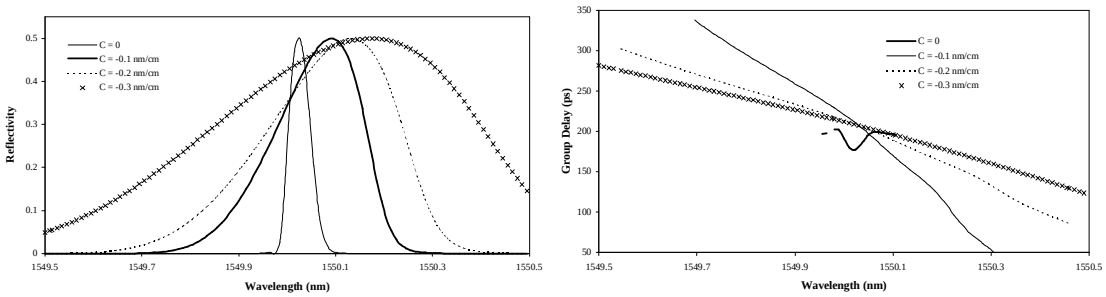

(a) (b)

Fig. 5. (a) Reflectivity and (b) group delay characteristics for the gratings with different values of linear chirp. The gratings are Gaussian apodized and 4 cm long.

The effect of the chirp on the reflection spectrum of a 4 cm long grating is given in Fig. 5(a). The peak reflectivity is taken as 0.5 as in Fig. 4 and the κ_p of the grating is calculated by the model. When the grating is unchirped, the reflection spectrum is narrow (FWHM = 0.5 Å) with a small side lobe on the short wavelength side. Although the pitch of the grating is not chirped for $C = 0$, there still exists some inherent "intrinsic" self-chirp because of the background refractive index variation (Gaussian in our case). This effective index variation causes the asymmetrical spectrum [9] as opposed to the symmetrical spectrum for uniform gratings [7]. As the magnitude of the chirp is increased, the spectrum becomes wider and the side lobe disappears [16]. FWHMs of the spectrum are 2.1 Å, 4.2 Å and 6.3 Å for the chirp rates of -1, -2 and -3 Å/cm, respectively. Although the unchirped reflector shows a sharper filter response, it does not allow an operation for a wide mode-locking frequency range in HSPS applications. This is an important feature for mode locking applications since the device can be mode-locked over a wide frequency range without physically changing the length of the grating. As the chirp rate is increased, the peak of the reflection spectrum is shifted towards the long wavelength side. The peak is located at 1550.03 nm for the grating with no chirp and shifted to 1550.095 nm, 1550.145 nm and 1550.175 nm for the chirp rates of -1, -2 and -3 Å/cm, respectively. This shift is due to the same reason explained for Fig. 2. That is, the increase in the chirp rate results in the increased averaged (effective) index change. The group delay characteristics of the fiber Bragg grating is found to change with the chirp rate as in Fig. 5(b). The side lobe shown in the reflection spectrum of the unchirped grating results in a discontinuity in the group delay curve [9]. Although the group delay curve for the unchirped reflector is nonlinear, it becomes linear as the rate of chirp is increased. Therefore, the higher chirp values will result in good gratings for HSPS applications.

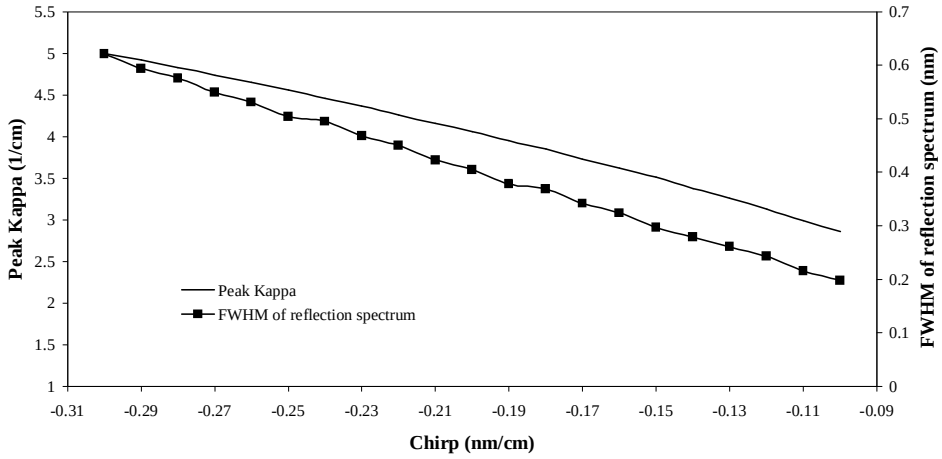

Fig. 6. The change in the FWHM of reflection spectrum and the κ_p with the chirp rate.

The peak of the refractive index change amplitude (κ_p) and the FWHM of the reflection spectrum as a function of the chirp rate are given in a more understandable form in Fig. 6. The peak κ is adjusted to give a peak reflectivity of 0.5 for each solution. Both curves show a linearly increasing trend with respect to the amount of chirp (magnitude). This is a result of the linear chirp incorporated in the grating.

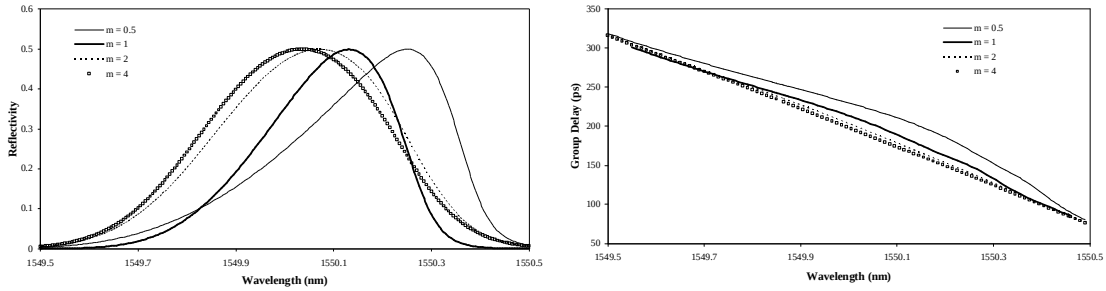

(a) (b)

Fig. 7. (a) Reflectivity and (b) group delay characteristics for the gratings with different modulation index values. The gratings are Gaussian apodized, linearly chirped (C = -0.2 nm/cm) and 4 cm long.

The effect of modulation index on the reflection spectrum is shown in Fig. 7(a). Higher modulation index values result in a more symmetric spectrum and a decrease on the shift of the resonance peak. This is due to the fact that the effect of averaged index decreases as the modulation index increases. At higher m values, the effect of the "ac" index change dominates the "dc" part since m is the ratio of the former to the latter. In this case grating behaves as if it only has an "ac" index variation. In other words, the grating shows a performance similar to that of an unapodized grating (see, for example, the case when m = 4). There is no side lobe in the reflection spectrum for any m value since the grating is chirped. The group delay characteristics for different m values are shown in Fig. 7(b). Although there are no big differences between the curves, the group delay curve for m = 0 is distorted most [8] due to the effect of the increased averaged refractive index.

4. Conclusions

We reported possible specifications of the fiber Bragg reflectors for mode-locked HSPS applications. It is shown in Fig. 2(a) that the grating without chirp produces side lobes at the reflection spectrum. Although the amplitudes of these lobes become smaller for weaker gratings, they do not disappear completely unless the pitch of the grating is chirped. The length of the grating can be changed in order to adjust the spectral width of the reflection spectrum as shown in Fig. 4(a). Even if the length of the grating is constant, its reflection spectrum can be made wider or narrower with the application of a proper amount of chirp as shown in Fig. 5. Finally, the reflection spectrum can be made symmetrical and its peak can be shifted by choosing proper values of m as given in Fig. 7. All these parameters are used to tailor the response of the grating and their optimum configuration can be found.

In this work, the coupled-mode equations are derived directly from the nonlinear index profile that contains a chirp term different than those given in the literature. The solutions of these equations and some results obtained from the model are compared with the results given in the literature. It is shown that both the equations and the results obtained from the model are in a good agreement.

As a result, it is found that the grating must be linearly chirped, and its length and index change must be adjusted according to the required specifications for HSPS applications. For instance, the length of the grating must be at least 3 cm if the chirp rate is –1 Å and the peak reflectivity is 0.5.

References

[1] P. A. Morton, V. Mizrahi, P. A. Andrekson, T. Tanbun-Ek, R. A. Logan, P. Lemaire, D. L. Coblentz, A. M. Sergent, K. W. Wecht, P. F. Sciortino Jr, IEEE Photon. Technol. Lett. **5**, 28 (1993).

[2] R. S. Tucker, U. Koren, G. Raybon, C. A. Burrus, B. I. Miller, T. L. Koch, G. Eisenstein, Electron. Lett. **25**, 621 (1989).
[3] P. A. Morton, J. E. Bowers, L. A. Kozsi, M. Soler, J. Lopata, D. P. Wilt, Appl. Phys. Lett. **56**, 111 (1990).
[4] M. S. Ozyazici, P. A. Morton, L. M. Zhang, V. Mizrahi, IEEE Photon. Technol. Lett. **7**, 1142 (1995).
[5] P. A. Morton, V. Mizrahi, G. Harvey, L. Mollenaur, T. Tanbun-Ek, R. A. Logan, H. M. Presby, T. Erdogan, A. M. Sergent, K. W. Wecht, IEEE Photon. Technol. Lett. **7**, 111 (1995).
[6] V. Mizrahi, J. E. Sipe, J. Lightwave Technol. **11**, 1513 (1993).
[7] T. Erdogan, J. Lightwave Technol. **15**, 1277 (1997).
[8] D. E. Pastor, J. Capmany, D. Ortega, V. Tatay, J. Marti, J. Lightwave Technol. **14**, 2581 (1996).
[9] L. G. Chen, S. D. Benjamin, P. W. E. Smith, J. E. Sipe, J. Lightwave Technol. **15**, 1503 (1997).
[10] W. H. Loh, M. J. Cole, M. N. Zervas, S. Barcelos, R. I. Laming, Opt. Lett. **20**, 2051 (1995).
[11] H. Kogelnik, In Tamir T (Ed.), Guided - Wave Optoelectronics, Springer Verlag, New York, 1990.
[12] J. Buus, SPIE Optical Engineering Press, Washington, 1991.
[13] J. E. Sipe, L. Poladian, M. Sterke, J. Opt. Soc. Amer. A **11**, 1307 (1994).
[14] F. Oulette, J. Cliche, S. Gagnon, J. Lightwave Technol. **12**, 1728 (1994).
[15] A. Carballar, M. A. Muriel, J. Lightwave Technol. **15**, 1314 (1997).
[16] M. Sayin, M. S. Ozyazici, Proc. WFOPC'98, 148 (1998).